atmosphere

MDPI

Article

Impact of Cumulus Options from Weather Research and Forecasting with Chemistry in Atmospheric Modeling in the Andean Region of Southern Ecuador

Rene Parra

Instituto de Simulación Computacional (ISC-USFQ), Colegio de Ciencias e Ingenierías, Universidad San Francisco de Quito USFQ, Quito 170901, Ecuador; rrparra@usfq.edu.ec

Abstract: Cumulus parameterization schemes model the subgrid-scale effects of moist convection, affecting the prognosis of cloud formation, rainfall, energy levels reaching the surface, and air quality. Working with a spatial resolution of 1 km, we studied the influence of cumulus parameterization schemes coded in the Weather Research and Forecasting with Chemistry Version 3.2 (WRF-Chem 3.2) for modeling in an Andean city in Southern Ecuador (Cuenca, 2500 masl), during September 2014. To assess performance, we used meteorological records from the urban area and stations located mainly over the Cordillera, with heights above 3000 masl, and air quality records from the urban area. Firstly, we did not use any cumulus parameterization (0 No Cumulus). Then, we considered four schemes: 1 Kain–Fritsch, 2 Betts–Miller–Janjic, 3 Grell–Devenyi, and 4 Grell-3 Ensemble. On average, the 0 No Cumulus option was better for modeling meteorological variables over the urban area, capturing 66.5% of records and being the best for precipitation (77.8%). However, 1 Kain–Fritsch was better for temperature (78.7%), and 3 Grell–Devenyi was better for wind speed (77.0%) and wind direction (37.9%). All the options provided acceptable and comparable performances for modeling short-term and long-term air quality variables. The results suggested that using no cumulus scheme could be beneficial for holistically modeling meteorological and air quality variables in the urban area. However, all the options, including deactivating the cumulus scheme, overestimated the total amount of precipitation over the Cordillera, implying that its modeling needs to be improved, particularly for studies on water supply and hydrological management. All the options also overestimated the solar radiation levels at the surface. New WRF-Chem versions and microphysics parameterization, the other component directly related to cloud and rainfall processes, must be assessed. In the future, a more refined inner domain, or an inner domain that combines a higher resolution (less than 1 km) over the Cordillera, with 1 km cells over the urban area, can be assessed.

Keywords: Cuenca; convective parameterization; cumulus convective; rainfall

check for updates

Citation: Parra, R. Impact of Cumulus Options from Weather Research and Forecasting with Chemistry in Atmospheric Modeling in the Andean Region of Southern Ecuador. *Atmosphere* **2024**, *15*, 693. https://doi.org/10.3390/atmos15060693

Academic Editor: Jimy Dudhia

Received: 7 April 2024
Revised: 22 May 2024
Accepted: 1 June 2024
Published: 6 June 2024

Copyright: © 2024 by the author. Licensee MDPI, Basel, Switzerland. This article is an open access article distributed under the terms and conditions of the Creative Commons Attribution (CC BY) license (https://creativecommons.org/licenses/by/4.0/).

1. Introduction

Air quality results from the complex interaction between atmospheric emissions and meteorology [1]. For atmospheric modeling purposes, cumulus convection is a component typically parameterized. It is directly related to cloud formation and, therefore, to solar radiation and temperature at the surface, affecting other variables such as the planetary boundary layer depth and atmospheric stability.

Complex topography and land-use heterogeneity, as in the Andean Region of Ecuador, directly affect the atmospheric dynamic [2], implying atmospheric modeling is challenging. For these cases, modeling with a spatial resolution of 1 km improves the topography and land-use representation. Atmospheric modeling was performed in Cuenca, an Andean city in southern Ecuador (2500 masl, Figure 1), using this spatial resolution to study the influence of planetary boundary layer schemes and to assess the impact on air quality of the shift from diesel to electric buses and the influence of feedback between aerosols and

meteorology. Recently, schemes for modeling the interaction near the land–atmosphere interface were assessed through land surface schemes [3].

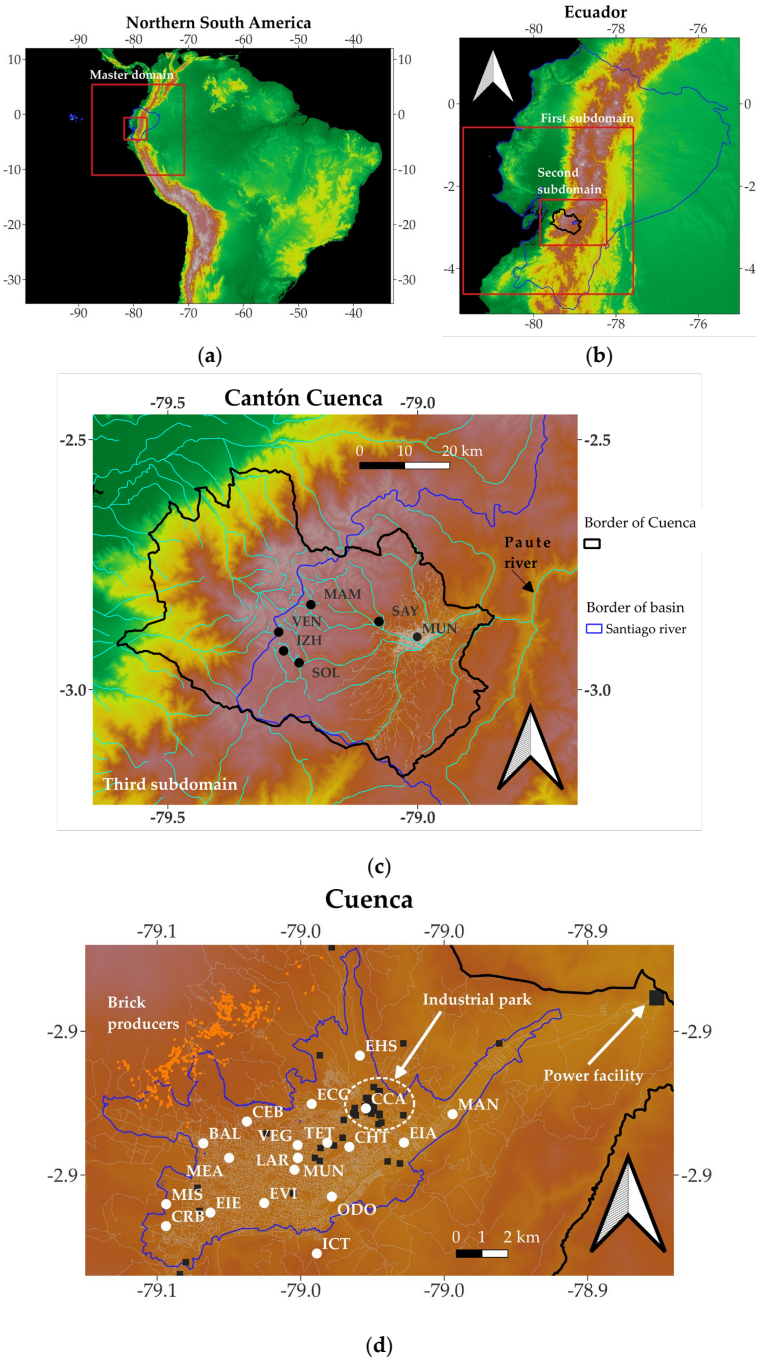


Figure 1. (**a**–**c**) Location of Cuenca. (**d**) The urban area of Cuenca (blue border). Black dots in (**c**) indicate the location of meteorological stations. The air quality network is indicated as white dots in (**d**). Orange dots (northwest) indicate the artisanal brick producers. Black squares indicate industries. MUN is the automatic station located at the historic center. White dots indicate passive stations. Nomenclature of meteorological stations: Izhcairrumi, IZH; Municipio, MUN; Mamamag, MAM; Sayausí, SAY; Soldados, SOL; and Ventanas, VEN. Nomenclature of air quality stations: BAL, Balzay; BCB, Bomberos; CCA, Colegio Carlos Arízaga; CEB, Cebollar; CHT, Colegio Herlinda Toral; CRB, Colegio Rafael Borja; ECC, Escuela Carlos Crespi; EHS, Escuela Héctor Sempértegui; EIA, Escuela Ignacio Andrade; EIE, Escuela Ignacio Escandón; EVI, Escuela Velasco Ibarra; ICT, Ictocruz; LAR, Calle Larga; MAN, Machángara; MEA, Mercado El Arenal; MIS, Misicata; MUN, Municipio; ODO, Facultad de Odontología; TET, Terminal Terrestre; and VEG, Vega Muñoz.

Clouds are relevant in Ecuador due to convective movements produced by the influence of the Intertropical Converge Zone (ITCZ) and the breeze coming from the coastal and Amazonian regions. Previous contributions identified options for improving atmospheric modeling in this region. Although acceptable performances were achieved, solar radiation at the surface was overestimated, and therefore, other components, such as the cumulus options, deserve dedicated studies.

Cumulus schemes model the sub-grid-scale effects of convective and shallow clouds. They represent the vertical fluxes due to unresolved updrafts and downdrafts and compensate for motion outside the clouds. Operating on individual columns, they provide vertical heating and moistening profiles. Some schemes offer column cloud and precipitation field tendencies [4].

Cumulus parameterizations are theoretically only valid for coarser grid sizes (e.g., greater than 10 km), which are necessary to properly release latent heat on a realistic time scale in the convective columns. While the assumptions about the convective eddies being entirely sub-grid-scale break down for finer grid sizes, sometimes these schemes have been found to help trigger convection in 5–10 km grid applications. The horizontal resolution of 1 km corresponds to the "grey zone", a range that might not require modeling with cumulus convective parameterization [5]. Modeling in the grey zone allows researchers to address whether working with higher resolution is always better [6], which is currently a line of active research in atmospheric science. Chow et al. (2019) reviewed the limitations of convective schemes in reproducing observed precipitation when modeling in the grey zone [2].

The Weather Research and Forecasting with Chemistry model (WRF-Chem V3.2) offers four schemes (Table 1) for modeling cumulus effects [4]. Cumulus schemes use different approaches and perform best when the assumptions are better satisfied; therefore, they must be assessed [7]. The Kain–Fritsch scheme [8] uses a simple cloud model with moist updrafts and downdrafts, including the effects of detrainment and entrainment and relatively simple microphysics. The Betts–Miller–Janjic option [9,10] considers as a variable the deep convection profiles and the relaxation time, depending on the cloud efficiency, which is a function of the entropy change, precipitation, and mean temperature of the cloud. The shallow convection moisture profile is based on the entropy change, which must be small and nonnegative. The Grell–Devenyi option [11] is an ensemble scheme using multiple cumulus models and variants within each grid box. The results are averaged to give feedback to the model. All the schemes are mass-flux types but have different updraft and downdraft entrainment and detrainment parameters and precipitation efficiencies. The dynamic control closures are based on the convective available potential energy, low-level vertical velocity, or moisture convergence. The Grell-3 scheme [11,12] has features in common with the Grell and Devenyi scheme, in the same way, based on an ensemble approach, but the quasi-equilibrium approach is not included among the scheme members. The scheme allows the subsidence effects to spread to neighboring grid columns, making the method more suitable for smaller grid sizes than 10 km. It can also be used at larger grid sizes where subsidence occurs within the same grid column as the updraft.

Table 1. Cumulus options in the WRF-Chem V3.2, based on [4].

Option	Nomenclature	Cloud Detrainment	Type	Closure
0	0 No Cumulus			
1	1 Kain–Fritsch	Yes	Mass flux	Convective Available Potential Energy (CAPE) removal
2	2 Betts–Miller–Janjic	No	Adjustment	Sounding adjustment
3	3 Grell–Devenyi	Yes	Mass flux	Various
5	4 Grell-3	Yes	Mass flux	Various

Cloud microphysics is the other component in which clouds occur on the scales of cloud droplets and hydrometeors [9]. It models precipitation on the grid scale, which plays an essential role in modeling moist convection [13]. Due to its scale, microphysical processes are always parameterized.

The atmospheric modeling coupling meteorology and air quality within one integrated approach evolved over the last years, recognizing that meteorology strongly influences air quality, and weather and climate are affected by changes in atmospheric composition [14]. Therefore, this contribution addresses the questions arising due to the use of WRF-Chem V3.2 in Cuenca:

- What cumulus parameterization scheme performs best for modeling meteorological and air quality?
- What is the effect of modeling without cumulus parameterization?
- What is the recommended option for holistically modeling meteorological and air quality variables?

2. Methods

2.1. The Air Quality Network

Cuenca has an air quality network working since 2008. In 2012, an automatic station was added to measure, in real-time, both air quality and meteorological variables in the historic center (MUN station, Figure 1), based on the national regulation requirements. Between 2012 and 2022, this station measured fine particulate matter ($PM_{2.5}$) yearly mean concentrations ranging between 5.7 and 14.5 μg m^{-3} [15], which are higher than the current World Health Organization (WHO) recommendation (5.0 μg m^{-3}) [16]. Moreover, during 116 days in 2022, the $PM_{2.5}$ 24 h mean levels were higher than the current WHO guideline (15 μg m^{-3}). In addition, during 7 days in 2022, the ozone (O_3) levels were higher than the WHO guideline (100 μg m^{-3}, maximum daily mean during 8 consecutive hours) [15,16]. In September, higher O_3 concentrations in Cuenca occurred, partly due to the high solar radiation levels at the surface, which promote O_3 production. Carbon monoxide (CO) is another pollutant measured at the MUN station.

The city also has passive stations for measuring mean monthly levels of nitrogen dioxide (NO_2) and O_3 (Figure 1d). Passive stations continuously collect air pollutants based on the principles of diffusion, the movement and spread of molecules across a concentration gradient [17]. EMOV EP (Spanish acronym for Empresa Pública Municipal de Movilidad, Tránsito y Transporte de Cuenca) is the municipal entity responsible for traffic and mobility activities and operates the air quality network. Records from the MUN and passive stations were used to assess the air quality modeling performance.

2.2. Meteorological Stations

Apart from air quality parameters, the MUN station measures the following meteorological variables: surface temperature, global solar radiation, wind speed, wind direction, and rainfall. These records were used to assess the modeling performance over the urban area.

In addition, we used records from five meteorological stations located west of the urban area, mainly over the Cordillera (Figure 1c). These stations are operated by ETAPA EP (Spanish acronym for Empresa Pública Municipal de Telecomunicaciones, Agua Potable, Alcantarillado y Saneamiento) in charge of the water supply and wastewater management. Four of these stations are located at heights over 3000 masl. Table 2 summarizes their main features and the parameters used in this study.

All the meteorological stations are located in the hydrological basin of the Paute River (Figure 1c), which is affluent of the Santiago River in the Amazonian region.

Table 2. Meteorological stations and parameters used in this study.

Station	Nomenclature	Entity	masl	Parameters
Municipio	MUN	EMOV EP	2582	Temperature, wind speed and direction, solar radiation, rainfall
Sayausí	SAY	ETAPA EP	2622	Temperature, rainfall
Mamamag	MAM	ETAPA EP	3609	Temperature, rainfall
Ventanas	VEN	ETAPA EP	3944	Temperature, rainfall
Izhcairrumi	IZH	ETAPA EP	3018	Temperature, rainfall
Soldados	SOL	ETAPA EP	3466	Temperature, rainfall

2.3. Emission Inventory of Cuenca

Speciated hourly emission maps deduced from the emission inventory 2014 [18] were used for previous atmospheric studies [3,19] that identified parameterization options for obtaining acceptable modeling performances in Cuenca. To complement these studies, other components, such as the cumulus options and related processes, require improvement and deserve a dedicated assessment.

The emission inventory 2014 reported that on-road traffic was the main source of pollutants (94.9% of CO, 71.2% of NO_x, 42.4% of $PM_{2.5}$, and 39.6% of NMVOC) [18]. Other NMVOC-important sources were solvents (29.7%) and vegetation (19.5%). Industries (Figure 1d) were the primary source of SO_2 (60.1%). About 600 artisan brick producers generated 38.5% of the $PM_{2.5}$ emissions. Also, a power facility generated 35.1% of SO_2 and 18.5% of NO_x emissions. From on-road traffic emissions, gasoline vehicles were the main contributors of CO and NMVOC, and diesel vehicles were the primary source of NO_x and $PM_{2.5}$.

2.4. Modeling Approach

Consistent with previous studies, we used the WRF-ChemV3.2 to model atmospheric parameters in September 2014, as O_3 levels are typically the highest in this region during this month. The WRF-Chem is a deterministic Eulerian 3-D atmospheric model used for research and forecasting [20]. It allows the simulation of the chemical transport of pollutants and the dynamic of atmospheric variables simultaneously. It also allows the activation of interactions between meteorological and air quality.

Figure 1 depicts the domains for modeling. The third and inner subdomain, formed by a grid of 100 × 82 cells, 1 km on each side, covering the territory of Cuenca (Figure 1c), was used to model meteorological and air quality variables. To generate the initial and boundary conditions, we selected the Global Operational Analysis (Final, FNL), provided by NCEP [21]. The Carbon Bond Mechanism Z (CBMZ) [22] and the MOSAIC (4 sectional aerosol bins) [23] were selected to speciate and represent, respectively, the corresponding hourly speciated emissions. Table 3 shows the schemes and options chosen for this contribution.

Table 3. Schemes and options selected for atmospheric modeling.

Component	Option	Model and References
Cumulus Parameterization	0	0 No Cumulus
	1	1 Kain–Fritsch [8]
	2	2 Betts–Miller–Janjic [9,10]
	3	3 Grell–Devenyi [11]
	5	4 Grell-3 [11,12]
Microphysics	4	WRF Single–moment 5–class [24]
Longwave Radiation	1	RRTM [25]

Table 3. *Cont.*

Component	Option	Model and References
Shortwave Radiation	2	Goddard [26]
Surface Layer	1	MM5 similarity [27]
Planetary Boundary Layer	1	Yonsei University [28]
Chemical mechanism and aerosol modules	7	CBMZ and MOSAIC [22,23]
Land Surface	2	Noah [29]
Urban surface	0	No urban physics

2.5. Metrics for Modeling Performance

We used the gross error (GE), mean bias (MB), and index of agreement (IOA) (Table 4) to assess the surface temperature modeling performance. We used the root mean square error (RMSA), MB, and IOA for wind speed. For wind direction, GE and MB were used. The expressions of these statistics can be found in the technical guide by the European Environment Agency (2011) [30] and in Simon et al. (2012) [31]. The performance for rainfall modeling was assessed through the Equation (1) metric.

$$Pdcm = \frac{Ndr + Ndwr}{Tmd} \times 100 \quad (1)$$

Pdcm: Percentage of days captured by modeling.
Ndr: Number of days with rainfall ($\geq$0.2 mm d^{-1}) captured by modeling.
Ndwr: Number of days without rainfall (<0.2 mm d^{-1}) captured by modeling.
Tmd: Total modeled days.

Table 4. Metrics for modeling atmospheric variables [30,31].

Variable	Metric	Benchmark or Ideal Range	Accuracy
Hourly surface temperature	GE MB IOA	<2 °C (−0.5 °C, 0.5 °C) ≥0.8	±2 °C
Hourly wind speed (10 mas)	RMSE MB IOA	<2 m s^{-1} (−0.5 m s^{-1}, 0.5 m s^{-1}) ≥0.6	±1 m s^{-1}
Hourly wind direction (10 mas)	GE MB	<30° (−10°, 10°)	±30°
Daily air quality: Max. 1 h CO mean, max. 8 h CO mean, 24 h $PM_{2.5}$ mean, max. 8 h O_3 mean	MB RMSE FB MNB r	0 0 0 0 1	±50%
Monthly air quality: NO_2 and O_3			±30%

The intensity of 0.2 mm d^{-1} corresponds to a day with measurable precipitation [32]. We considered that the model captured the record for days without rainfall if the computed rainfall and the corresponding record were <0.2 mm d^{-1}. We considered that the model captured the corresponding record for days with rain if the computed rainfall and the corresponding record were ≥0.2 mm d^{-1}.

The WRF-Chem outputs obtained total modeled precipitation as the contribution of the cumulus parameterization (RAINC variable) and the cloud microphysics scheme

(RAINNC variable). The total rainfall during the study period provided by the cumulus options was compared to the corresponding records.

In addition, for the variables of Table 2, we obtained the percentages of records captured by modeling based on the maximum allowed deviation between the observed and modeled values of Table 4.

Finally, we compared the cloud coverage provided by the Terra satellite over Cuenca (10:30 LT) [33] with the global solar radiation at the surface to deduce the modeling's performance in capturing changes in solar radiation under the influence of clouds.

For short-term (daily) air quality, we used the records from the MUN station (Figure 1c,d) to assess the performance for modeling the CO, $PM_{2.5}$, and O_3 (Table 4) concentration, during periods established by the national regulation and the WHO guidelines [16,31,34], using the MB, RMSE, the fractional bias (FB), the mean normalized bias (MNB), and the correlation coefficient (r) [31].

For long-term (monthly) air quality, the performance was defined by the percentage of the passive stations (Figure 1d), showing a maximum difference of 30% between the computed concentration and the records.

3. Results

3.1. Meteorology

Although they overestimated temperatures between 13:00 and 17:00 (LT), all the cumulus options performed similarly when modeling surface temperature (Table 5), with GE (1.3 °C), MB (0.1–0.2 °C), and IOA (0.9) metrics within the corresponding value benchmark ranges, and they captured the behavior of the mean daily profile (Figure 2a). The hourly temperature was adequately modeled at the SAY, VEN, and IZH stations (GE < 2 °C, Table 6). In all the stations out of the urban area, there was a strong relationship between records and modeled temperatures (IOA ≥0.8). Over the Cordillera, no unique cumulus option provided the best performance for modeling temperature.

Table 5. Metrics for modeling meteorological variables. MUN station.

Cumulus Option:	0 No Cumulus	1 Kain–Fritsch	2 Betts–Miller–Janjic	3 Grell–Devenyi	4 Grell-3	Benchmark
Hourly surface temperature:						
GE	**1.3**	**1.3**	**1.3**	**1.3**	**1.3**	**<2 °C**
MB	**0.2**	**0.2**	**0.2**	**0.1**	**0.1**	**<±0.5 °C**
IOA	**0.9**	**0.9**	**0.9**	**0.9**	**0.9**	**≥0.8**
Hourly wind speed:						
RMSE	**1.0**	**1.0**	**1.0**	**0.9**	**0.9**	**<2 m s^{-1}**
MB	**0.4**	**0.4**	**0.4**	**0.2**	**0.2**	**<±0.5 m s^{-1}**
IOA	**0.8**	**0.8**	**0.8**	**0.9**	**0.9**	**≥0.6**
Hourly wind direction:						
GE	63.5	62.2	62.4	61.7	61.9	**<30°**
MB	−23.5	−23.5	−23.9	−20.5	−20.8	**<±10°**

The 3 Grell–Devenyi and 4 Grell-3 options reproduced the temperature better during the afternoon (Figure 2a), showing the lowest value of the MB (0.1 °C). In addition, the IOA (0.9) indicated a strong relationship between records and modeled temperatures for all the options. The 1 Kain–Fritsch scheme captured 78.7% of the temperature records (Table 7).

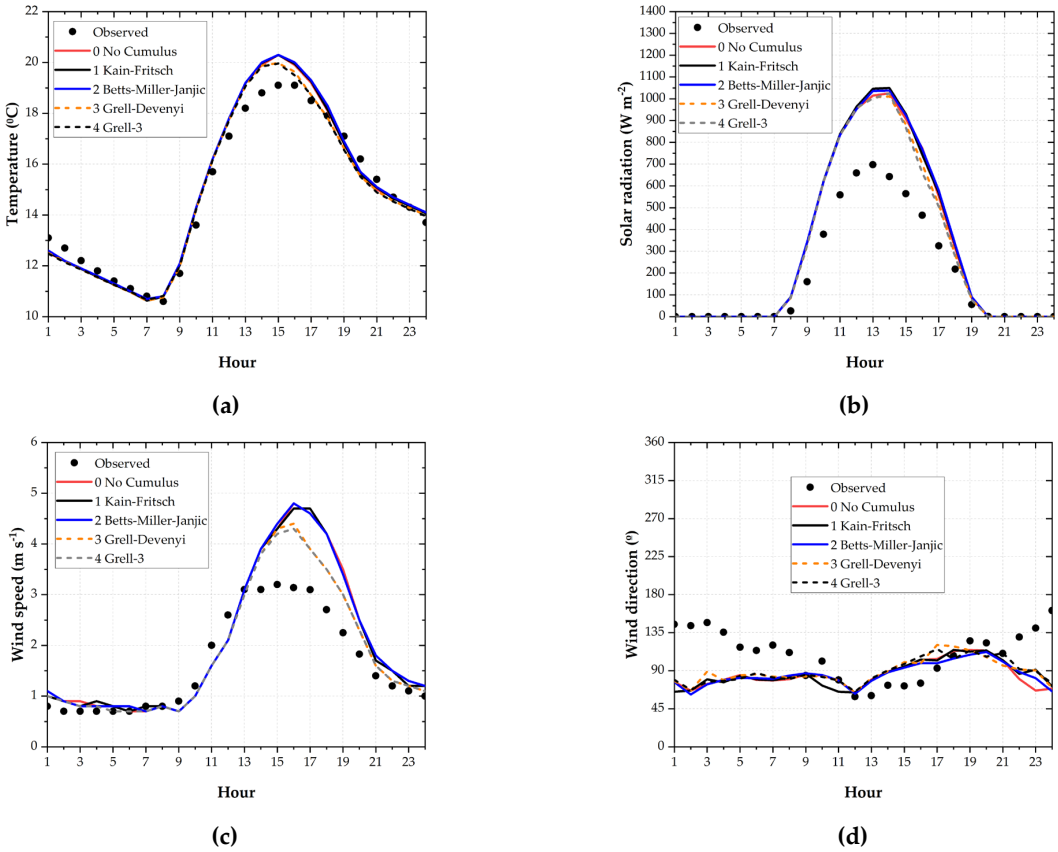


Figure 2. MUN station. Daily mean profiles during September 2014: (**a**) Temperature. (**b**) Global solar radiation. (**c**) Wind speed. (**d**) Wind direction.

Table 6. Metrics for modeling meteorological variables. Other stations.

Cumulus Option:	0 No Cumulus	1 Kain–Fritsch	2 Betts–Miller–Janjic	3 Grell–Devenyi	4 Grell-3	Benchmark
Hourly surface temperature: SAY station						
GE	**1.8**	**1.7**	**1.7**	**1.8**	**1.8**	**<2 °C**
MB	−1.2	−1.2	−1.2	−1.3	−1.3	**<±0.5 °C**
IOA	**0.9**	**0.9**	**0.9**	**0.9**	**0.9**	**≥0.8**
Hourly surface temperature: MAM station						
GE	2.0	2.0	2.0	2.0	2.0	**<2 °C**
MB	−1.8	−1.7	−1.7	−1.7	−1.7	**<±0.5 °C**
IOA	**0.8**	**0.8**	**0.8**	**0.8**	**0.8**	**≥0.8**
Hourly surface temperature: VEN station						
GE	**1.1**	**1.1**	**1.1**	**1.1**	**1.1**	**<2 °C**
MB	**0.0**	**0.1**	**0.1**	**0.0**	**0.0**	**<±0.5 °C**
IOA	**0.9**	**0.9**	**0.9**	**0.9**	**0.9**	**≥0.8**
Hourly surface temperature: IZH station						
GE	**1.2**	**1.2**	**1.2**	**1.2**	**1.2**	**<2 °C**
MB	**−0.2**	**−0.2**	**−0.1**	**−0.2**	**−0.2**	**<±0.5 °C**
IOA	**0.9**	**0.9**	**0.9**	**0.9**	**0.9**	**≥0.8**
Hourly surface temperature: SOL station						
GE	2.3	2.3	2.3	2.3	2.3	**<2 °C**
MB	−1.7	−1.7	−1.7	−1.8	−1.8	**<±0.5 °C**
IOA	**0.8**	**0.8**	**0.8**	**0.8**	**0.8**	**≥0.8**

Table 7. Records captured (percentage) by modeling. Meteorological variables. MUN station.

Cumulus Option:	0 No Cumulus	1 Kain–Fritsch	2 Betts–Miller–Janjic	3 Grell–Devenyi	4 Grell-3	Records
Hourly surface temperature	77.8	**78.7**	78.1	77.0	78.0	644
Hourly wind speed	73.9	74.1	73.8	**77.0**	76.9	644
Hourly wind direction	36.6	37.1	37.0	**37.9**	37.1	644
Daily rainfall	**77.8**	70.4	63.0	66.7	63.0	27
Average	**66.5**	65.1	62.9	64.6	63.7	

The metrics for modeling all the options were in the benchmark ranges for wind speed, although 3 Grell–Devenyi and 4 Grell-3 achieved the best performance (Table 7). While all the options overestimated the wind surface during the afternoon, these two schemes were the best (Figure 2c). The 3 Grell–Devenyi scheme captured the highest percentage (77.0%) of the wind speed records (Table 5).

None of the options provided metric values within the expected range (<30°) for wind direction. Wind direction was better modeled between 09:00 and 21:00 LT (Figure 2d). The 3 Grell–Devenyi, the option with the best GE (61.7°), captured only 37.9% of the wind speed records.

At the MUN station, the 0 No Cumulus option was the best for rainfall, providing the highest percentage (77.8%) of records captured by modeling, followed by 1 Kain–Fritsch (70.4%). No unique option was the best for modeling each of the four assessed meteorological parameters over the urban area. However, on average, the 0 No Cumulus option achieved the best percentage (66.5%), followed by the 1 Kain–Fritsch (65.1%) (Table 7).

At the MUN station, from 1 to 27 September 2014, 20 days showed no rainfall or intensities lower or equal to 0.2 mm d^{-1} (Figure 3). Five days showed records between 0.4 and 7.5 mm d^{-1} (11, 12, 16, 22, and 24 September 2014). On 13 and 15 September 2014, rainfall intensities were recorded at 11.7 and 13.6 mm d^{-1}, respectively. Figure 4c indicates that 0 No Cumulus and 1 Kain–Fritsch were better for modeling daily rainfall. The 3 Grell–Devenyi and 4 Grell-3 modeled more days with rain, although the corresponding records indicated the absence of precipitation (e.g., 18, 19, 20, 21, 23 September 2014, with rainfall between 7.4 and 23.4 mm d^{-1}).

Figure 4 depicts the modeled rainfall maps for 20 September 2014. As expected, the computed cumulus contribution to rainfall for the 0 No Cumulus option was null (Figure 4a). For the 1 Kain–Fritsch and 2 Betts–Miller–Janjic, the cumulus contribution reached up to 12 mm d^{-1}, mainly in places to the W of the urban area (Figure 4d,e). However, for the 3 Grell–Devenyi and 4 Grell-3, this contribution was up to 50 mm d^{-1}, mainly in the W, over the Cordillera (Figure 4j,m), where the convective contribution was higher compared to the 1 Kain–Fritsch and 2 Betts–Miller–Janjic schemes.

Figure 5 depicts the modeled rainfall maps for 22 September 2014. For the 1 Kain–Fritsch and 2 Betts–Miller–Janjic, the cumulus contribution reached 8 mm d^{-1}, mainly in the south and southwest of the urban area (Figure 5d,e). However, for the 3 Grell–Devenyi and 4 Grell-3, this contribution was up to 20 mm d^{-1}, mainly in the W, N, and S (Figure 5j,m). Over the Cordillera, the convective contribution was lower than the microphysics component for all the cumulus options.

No unique option was best for modeling daily rainfall outside the urban area (Table 8). At three stations located over the Cordillera (VEN, IZH, and SOL), all the cumulus options overestimated the total precipitation during the study period, with differences between 41.6 and 210.4% compared with records (Table 9).

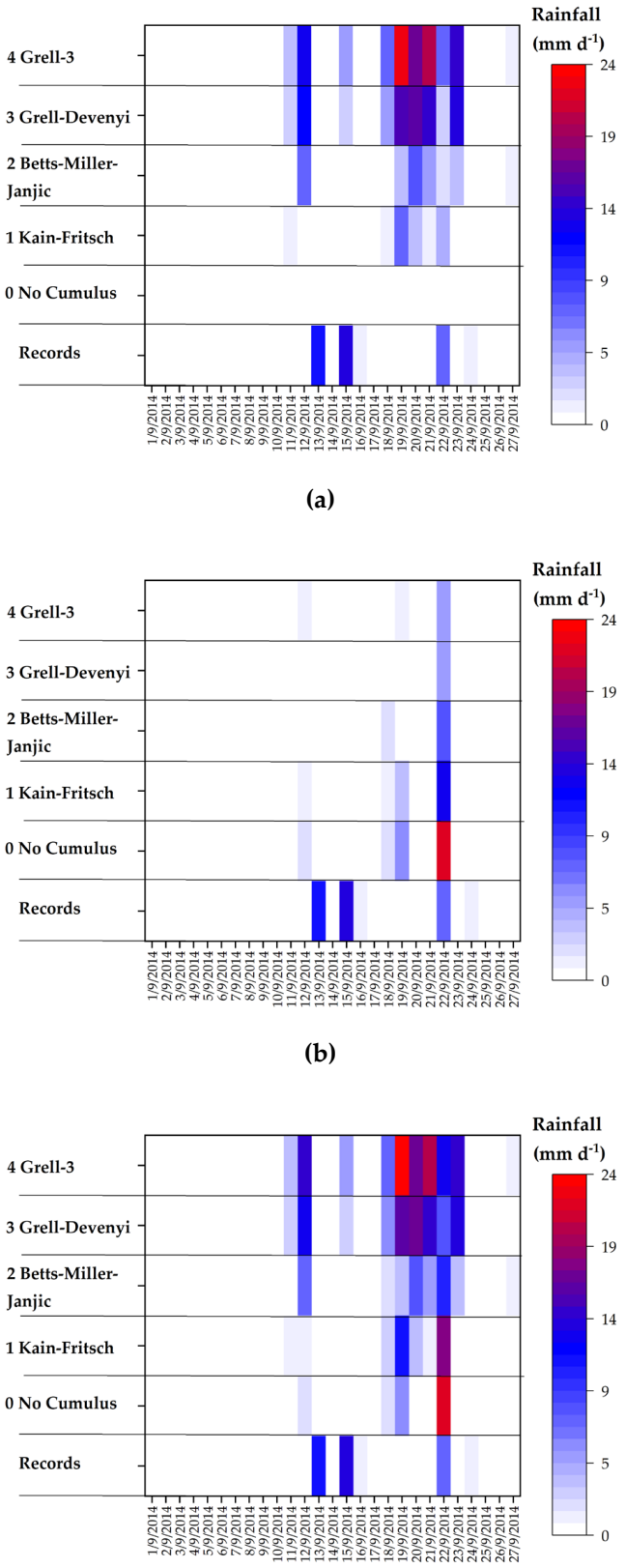


Figure 3. Rainfall records at the MUN station and modeled values (mm d^{-1}): (**a**) contribution of cumulus parameterization (RAINC variable from WRF-Chem), (**b**) contribution of microphysics (RAINNC variable from WRF-Chem), (**c**) cumulus and microphysics (RAINC and RAINNC).

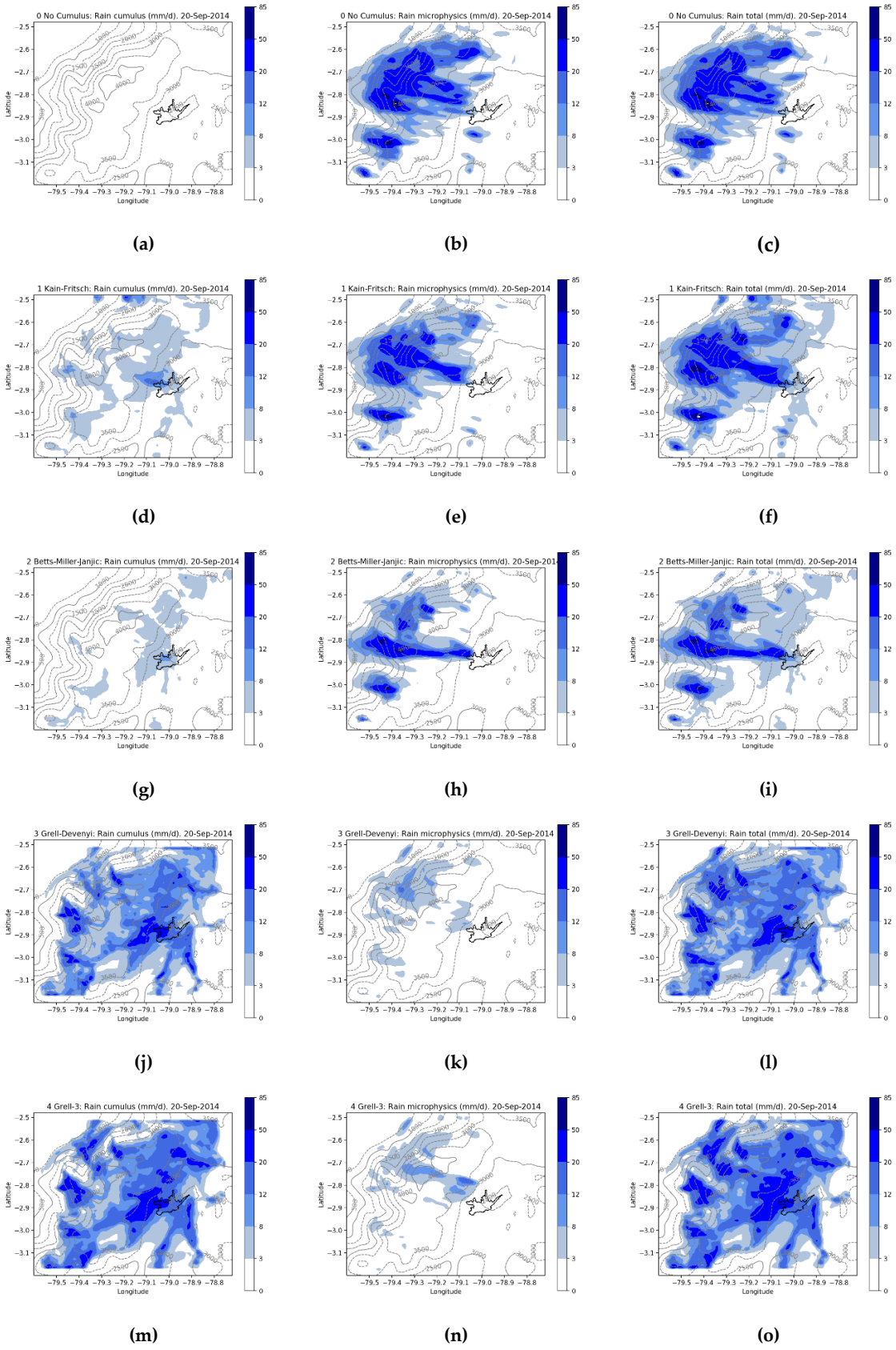


Figure 4. Modeled rainfall (mm d^{-1}) contribution from cumulus parameterization (RAINC), microphysics (RAINNC), and total (RAINC + RAINNC) for 20 September 2014: (**a**–**c**) 0 No Cumulus, (**d**–**f**) 1 Kain–Fritsch, (**g**–**i**) 2 Betts–Miller–Janjic, (**j**–**l**) 3 Grell–Devenyi, (**m**–**o**) 4 Grell-3.

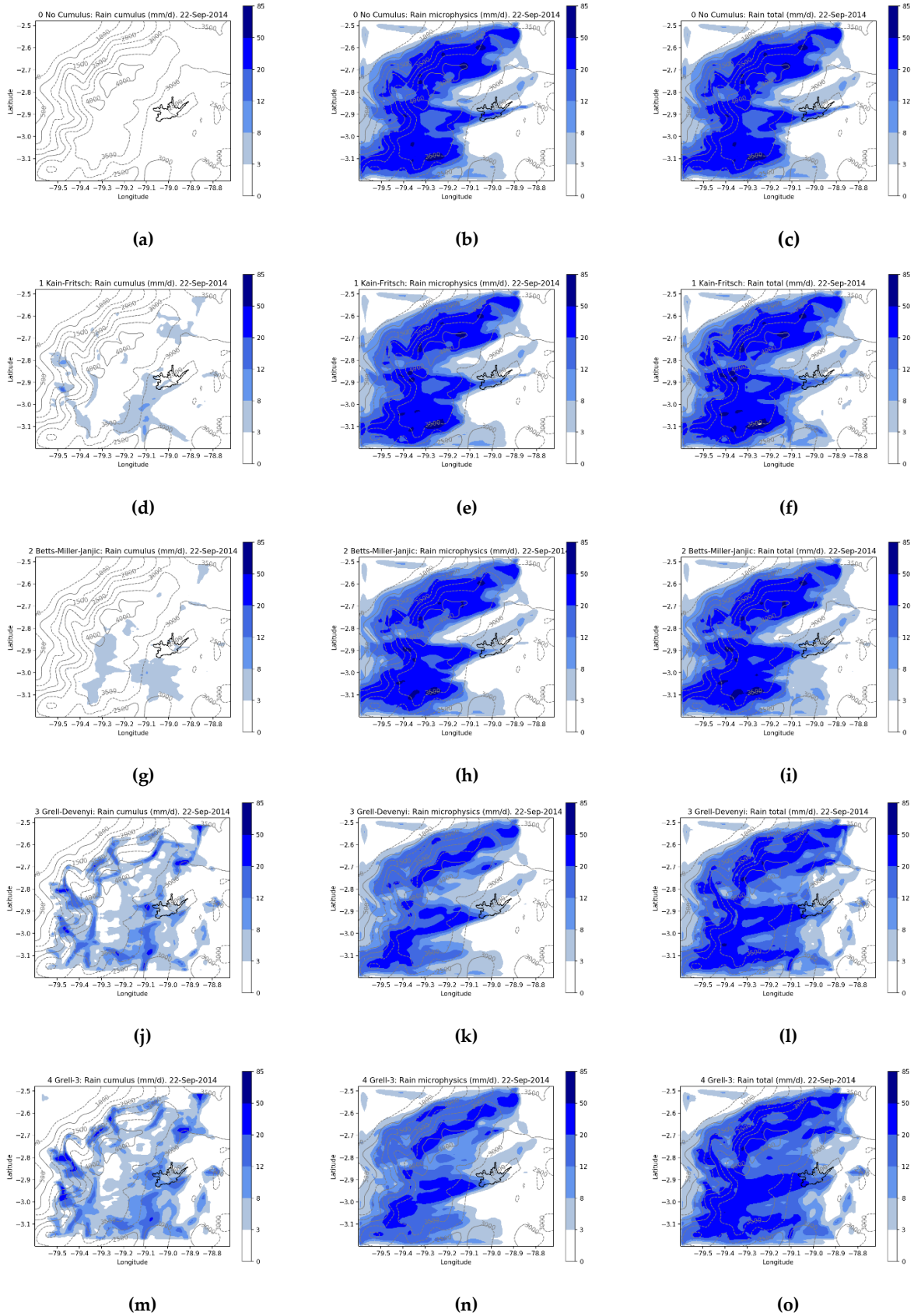


Figure 5. Modeled rainfall (mm d^{-1}) contribution from cumulus parameterization (RAINC), microphysics (RAINNC), and total (RAINC + RAINNC) for 22 September 2014: (**a**–**c**) 0 No Cumulus, (**d**–**f**) 1 Kain–Fritsch, (**g**–**i**) 2 Betts–Miller–Janjic, (**j**–**l**) 3 Grell–Devenyi, (**m**–**o**) 4 Grell-3.

Table 8. Temperature and precipitation records captured (percentage) by modeling.

Station	0 No Cumulus	1 Kain–Fritsch	2 Betts–Miller–Janjic	3 Grell–Devenyi	4 Grell-3	Records
Hourly surface temperature						
SAY	62.7	**63.2**	63.0	62.3	61.8	644
MAM	58.1	**60.1**	59.8	58.2	57.3	644
VEN	83.2	83.9	83.2	**85.4**	85.2	644
IZH	81.4	81.2	81.1	**82.0**	80.9	644
SOL	43.8	43.3	**46.1**	42.7	43.5	644
Daily rainfall						
SAY	**63.0**	59.3	55.6	**63.0**	**63.0**	27
MAM	59.3	**74.1**	63.0	55.6	63.0	27
VEN	**70.4**	**70.4**	63.0	66.7	66.7	27
IZH	59.3	55.6	48.1	**63.0**	**63.0**	27
SOL	74.1	66.7	**77.8**	74.1	66.7	27

Table 9. Rainfall records and modeled values from 1 to 27 September 2014. Bold numbers indicate the options with differences lower than 50%.

Station	Records	0 No Cumulus	1 Kain–Fritsch	2 Betts–Miller–Janjic	3 Grell–Devenyi	4 Grell-3
Total rainfall (records, mm)						
MUN	36.7	**31.9**	**39.4**	**42.7**	94.2	119.8
SAY	55.8	**39.7**	103.1	100.3	160.4	186.8
MAM	77.8	**108.5**	128.9	**81.8**	**110.5**	127.5
VEN	49.9	154.9	141.5	105.5	80.2	85.5
IZH	56.7	135.2	147.0	119.8	112.4	124.0
SOL	54.7	106.2	113.2	**77.4**	86.4	104.8
(Total modeled rainfall − Total rainfall)/(Total rainfall) × 100						
MUN		**−13.2**	**7.3**	**16.3**	156.6	226.3
SAY		**−28.8**	84.8	79.7	187.5	234.7
MAM		**39.4**	65.7	**5.2**	**42.0**	63.9
VEN		210.4	183.6	111.3	60.6	71.4
IZH		138.5	159.2	111.4	98.3	118.7
SOL		94.1	107.0	**41.6**	58.0	91.5

Appendix A shows imageries provided by the Terra satellite over Cuenca (10:30 LT) [33] suggested that during the study period, 5 days were cloudless, 13 were partially cloudy, and 4 were cloudy (Figures A1–A3). Table A1 shows the cloud conditions inferred from the remote-sensing data and each option's corresponding qualitative performance for modeling solar radiation. All the options, on average, overestimated the global solar radiation at the surface (Figure 2b).

3.2. Air Quality

Although there were slight differences, the 2 Betts–Miller–Janjic received better metrics for modeling the maximum CO daily 1 h mean, followed by the 0 No Cumulus option (Table 10). Similarly, the 0 No Cumulus, 3 Grell–Devenyi, and 4 Grell-3 presented better performance modeling of the CO daily 8 h mean concentrations.

Figures 6–8 compare observed versus modeled CO, $PM_{2.5}$, and O_3 records for all the cumulus options (a, b, c, d, e).

All the options provided consistent mean daily profiles of hourly concentrations (Figure 6f). The 0 No Cumulus (96.3%) and 1 Kain–Fritsch (96.3%) better captured the records of the maximum CO daily 1 h mean (Table 11).

Table 10. Short-term air quality metrics.

Cumulus Option:	0 No Cumulus	1 Kain–Fritsch	2 Betts–Miller–Janjic	3 Grell–Devenyi	4 Grell-3	Ideal Value
Maximum 1 h CO mean:						
MB	0.10	0.11	**0.08**	0.11	0.10	**0**
RMSE	0.55	0.55	**0.54**	0.57	0.56	**0**
FB	5.6	6.5	**4.6**	6.5	6.1	**0**
MNB	7.09	8.55	**6.35**	9.11	8.42	**0**
r	**0.47**	0.45	0.46	0.38	0.41	**1**
Maximum 8 h CO mean:						
MB	**−0.08**	**−0.08**	−0.09	**−0.08**	**−0.08**	**0**
RMSE	**0.20**	**0.20**	**0.20**	0.21	**0.20**	**0**
FB	−10.4	−10.2	−11.1	**−9.8**	−9.9	**0**
MNB	−9.56	−9.20	−10.04	**−8.67**	−8.81	**0**
r	**0.45**	0.43	0.43	0.38	0.39	**1**
24 h $PM_{2.5}$ mean:						
MB	1.02	1.05	**0.87**	1.17	1.17	**0**
RMSE	3.16	3.16	**3.10**	3.22	3.25	**0**
FB	14.9	15.2	**12.8**	16.8	16.8	**0**
MNB	41.76	42.19	**39.08**	44.95	45.73	**0**
r	0.07	0.06	0.05	0.04	0.01	**1**
Maximum 8 h O_3 mean:						
MB	15.86	15.92	16.09	**15.29**	**15.29**	**0**
RMSE	18.83	18.80	18.93	18.54	**18.51**	**0**
FB	24.1	24.2	24.4	**23.3**	**23.3**	**0**
MNB	31.50	31.61	31.92	**30.61**	**30.61**	**0**
r	0.26	0.28	0.28	**0.19**	0.20	**1**

Table 11. Records captured (percentage) by modeling. Air quality variables.

Cumulus Option:	0 No Cumulus	1 Kain–Fritsch	2 Betts–Miller–Janjic	3 Grell–Devenyi	4 Grell-3	Records
Short-term air quality:						
Max. 1 h CO mean	**96.3**	**96.3**	88.9	92.6	92.6	27
Max. 8 h CO mean	96.3	**100.0**	96.3	**100.0**	**100.0**	27
24 h $PM_{2.5}$ mean	**63.0**	**63.0**	**63.0**	**63.0**	**63.0**	27
Max. 8 h O_3 mean	81.5	81.5	81.5	**85.2**	**85.2**	27
Average:	84.3	**85.2**	82.4	**85.2**	**85.2**	
Long-term air quality:						
NO_2, monthly mean	**93.3**	**93.3**	**93.3**	**93.3**	**93.3**	15
O_3, monthly mean	**56.3**	**56.3**	**56.3**	**56.3**	**56.3**	16
Average:	**74.8**	**74.8**	**74.8**	**74.8**	**74.8**	

Similarly, with slight differences, the 2 Betts–Miller–Janjic received better metrics for modeling the 24 h $PM_{2.5}$ mean concentrations, followed by the 0 No Cumulus option (Table 10). All the options captured 63.0% of records (Table 11), providing similar mean daily profiles (Figure 7f).

For modeling the maximum 8 h O_3 daily mean, the 4 Grell-3 and 3 Grell–Devenyi options performed better, followed by the 0 No Cumulus (Table 10). The 3 Grell–Devenyi and 4 Grell-3 captured 85.2% of records (Table 11). On average, all the options overestimated the mean O_3 daily profile at midday and afternoon (Figure 8f).

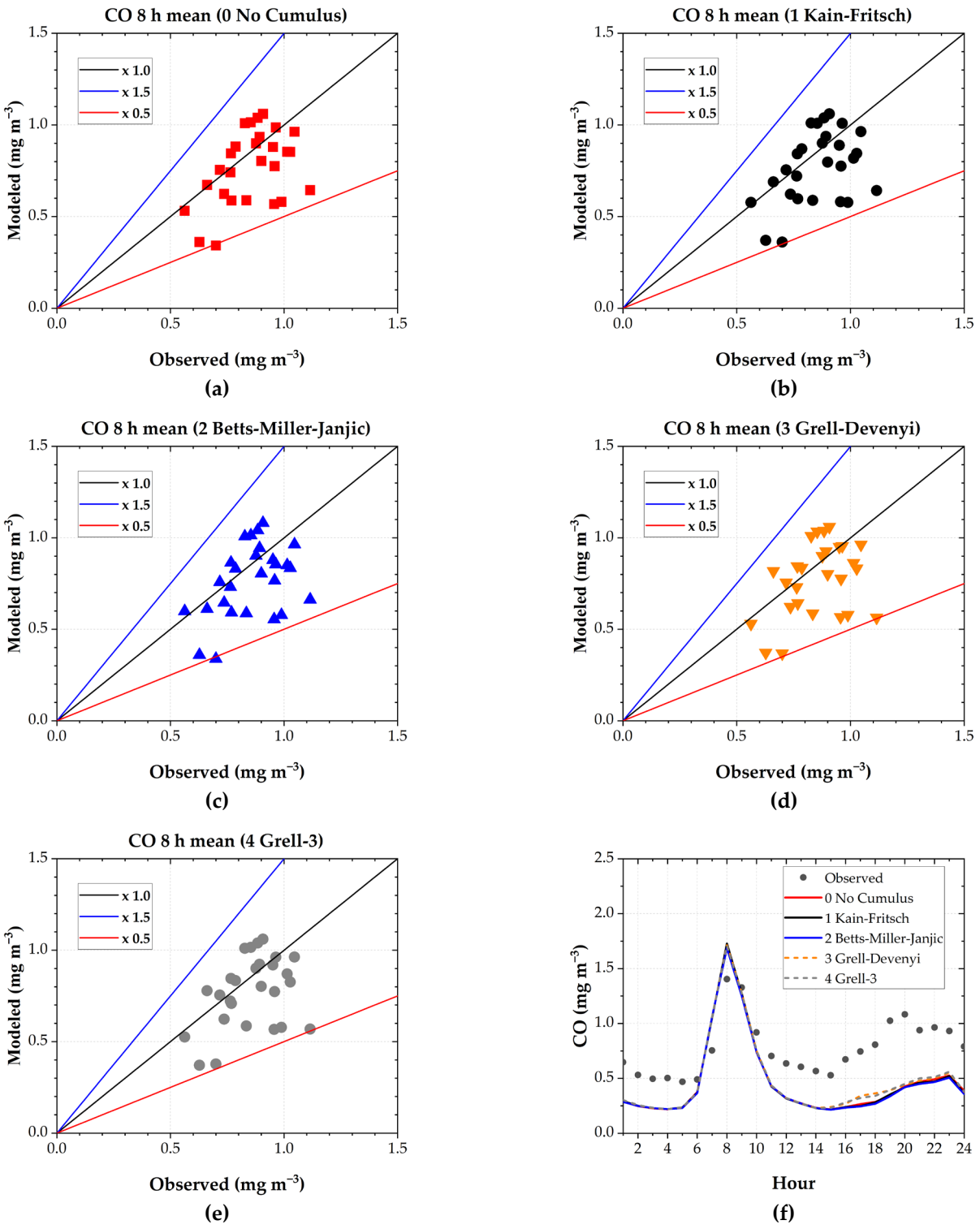


Figure 6. Observed versus modeled daily CO 8 h maximum: (**a**) 0 No Cumulus; (**b**) 1 Kain–Fritsch; (**c**) 2 Betts–Miller–Janjic; (**d**) 3 Grell–Devenyi; (**e**) 4 Grell-3. (**f**) Mean daily profiles of hourly CO concentrations. Black lines indicate the y = x equation (perfect fit). Blue and red lines indicate the expected accuracy ranges for modeling short-term air quality variables (±50%) based on the recommendation by the EEA [30].

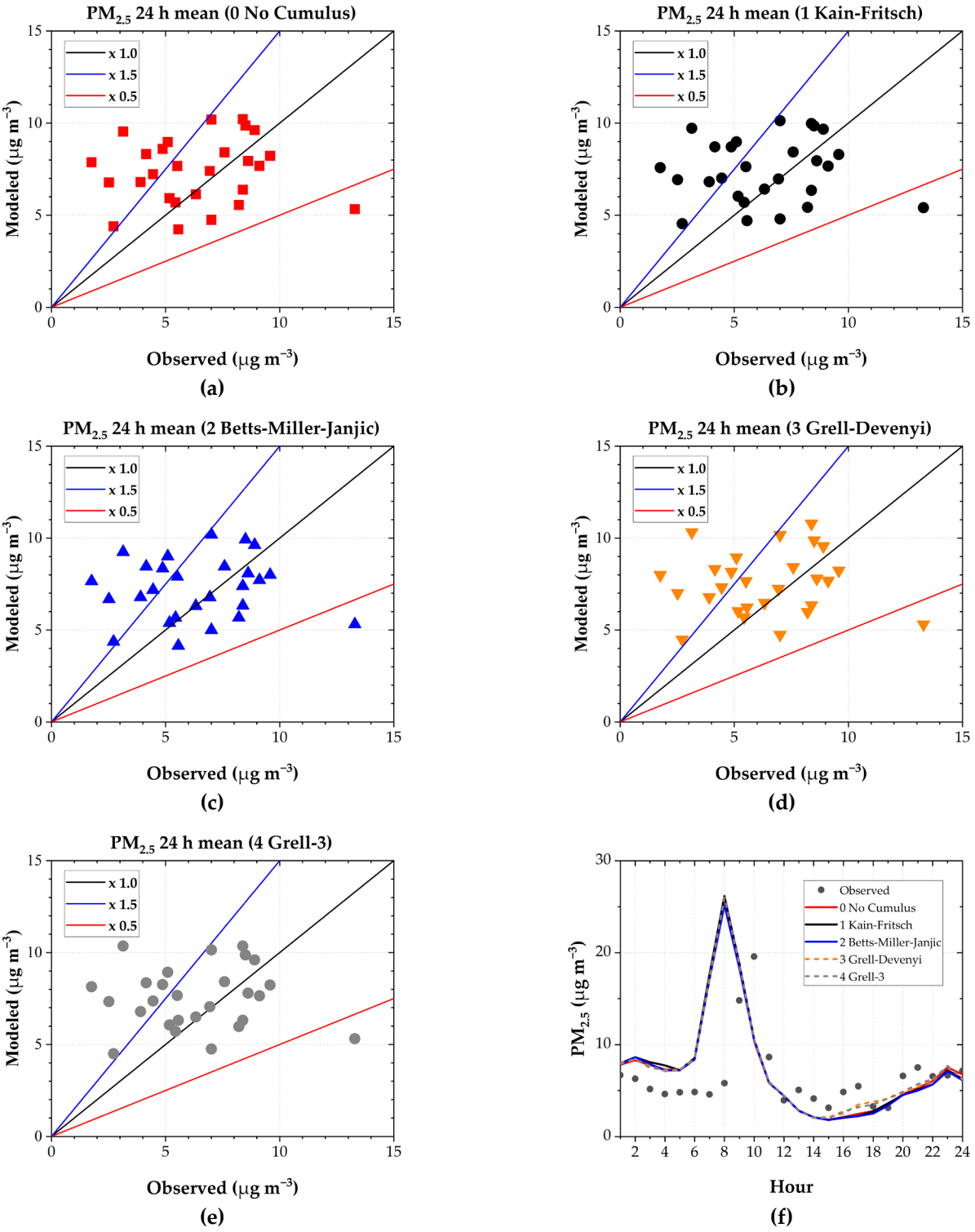


Figure 7. Observed versus modeled daily $PM_{2.5}$ 24 h mean: (**a**) 0 No Cumulus; (**b**) 1 Kain–Fritsch; (**c**) 2 Betts–Miller–Janjic; (**d**) 3 Grell–Devenyi; (**e**) 4 Grell-3. (**f**) Mean daily profiles of hourly $PM_{2.5}$ concentrations. Black lines indicate the y = x equation (perfect fit). Blue and red lines indicate the expected accuracy ranges for modeling short-term air quality variables (±50%) based on the recommendation by the EEA [31].

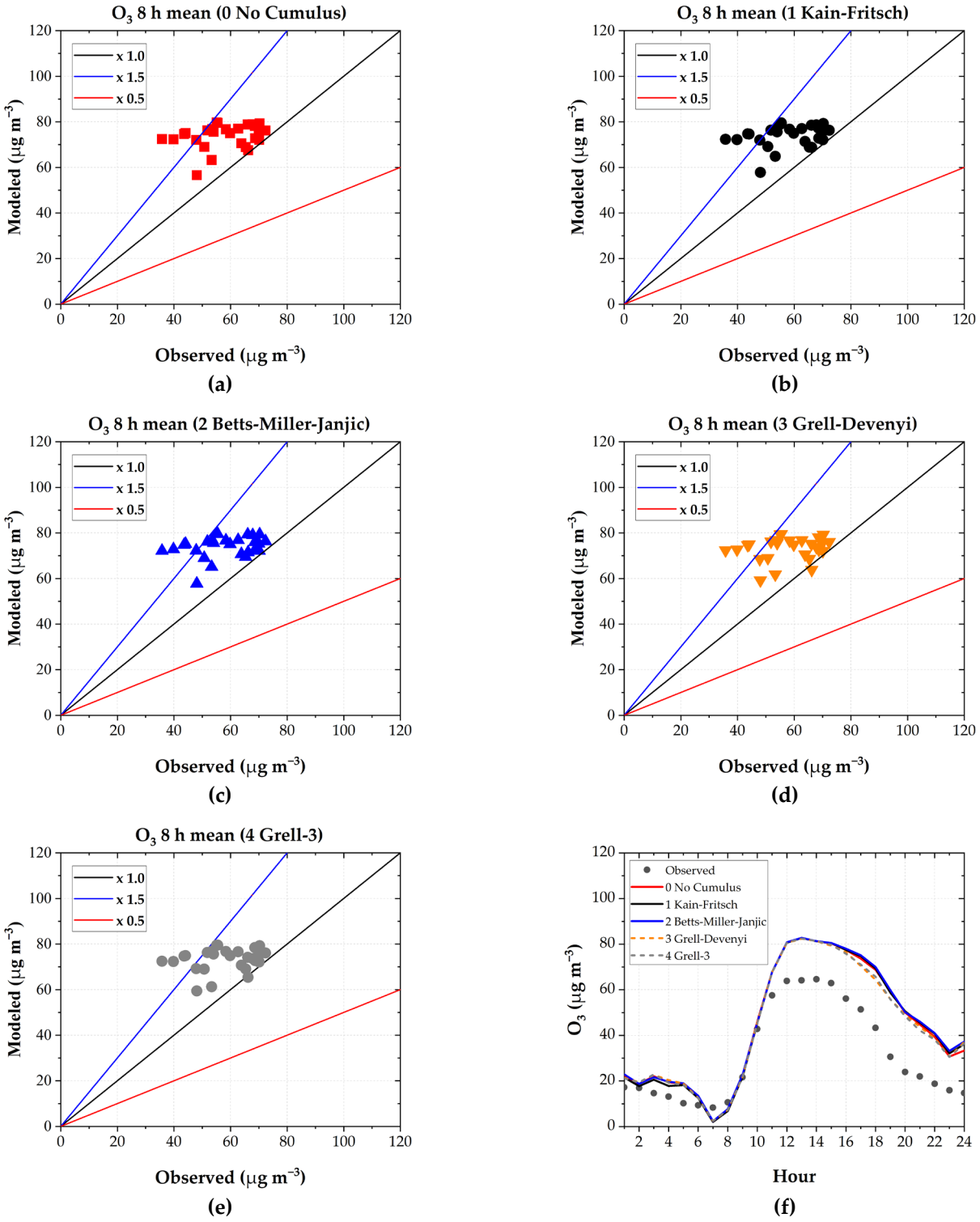


Figure 8. Observed versus modeled daily O_3 8 h maximum mean: (**a**) 0 No Cumulus; (**b**) 1 Kain–Fritsch; (**c**) 2 Betts–Miller–Janjic; (**d**) 3 Grell–Devenyi; (**e**) 4 Grell-3. (**f**) Mean daily profiles of hourly O_3 concentrations. Black lines indicate the y = x equation (perfect fit). Blue and red lines indicate the expected accuracy ranges for modeling short-term air quality variables (±50%) based on the recommendation by the EEA [31].

Regarding the NO_2 and O_3 monthly mean concentrations, all options performed similarly, capturing 93.3% and 56.3% of records, respectively (Table 11, Figure 9).

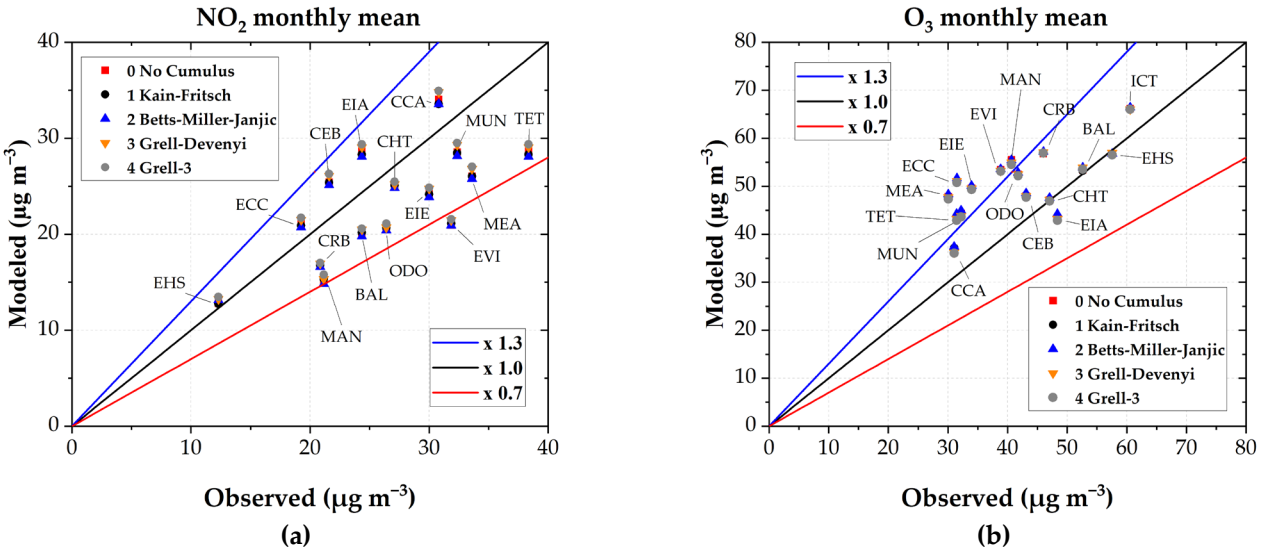


Figure 9. Observed versus modeled concentrations in passive stations: (**a**) NO_2 and (**b**) O_3. Black lines indicate the y = x equation (perfect fit). Blue and red lines indicate the expected accuracy ranges for modeling short-term air quality variables (±30%) based on the recommendation by the EEA [31].

4. Discussion and Conclusions

Applying the online approach, we used the WRF-Chem V3.2, a state-of-the-art atmospheric tool for modeling meteorological (surface temperature, wind speed, wind direction, rainfall) and air quality parameters (short-term: CO, $PM_{2.5}$, and O_3; long-term: NO_2 and O_3) in Cuenca, an Andean city in Southern Ecuador, in September 2014, a month when tropospheric O_3 concentrations are typically higher in the region. We made numerical experiments to assess the influence on the performance of the cumulus schemes coded in WRF-Chem V3.2 (Kain–Fritsch, Betts–Miller–Janjic, Grell–Devenyi, and Grell-3) and the option of modeling without cumulus parameterization, working with a spatial resolution of 1 km. This resolution corresponds to the grey zone, a range of 1 to 10 km for moist convection [6], whose length scale can be similar in size and potentially without the need for convective parameterization.

The results indicated that no unique option was the best for modeling each of the assessed variables over the entire inner domain, suggesting that using no cumulus scheme could be beneficial for holistically modeling meteorological and air quality variables in the urban area of Cuenca, where rainfall modeling improved through the deactivation of a cumulus scheme. Over the urban area, cumulus schemes provided better performances for temperature, wind speed, and wind direction than modeling with deactivation of cumulus parameterization. On the contrary, all the options overestimated the total amount of modeled rainfall over the Cordillera during the simulation period. All the options provided comparable modeling performances for short- and long-term simulations regarding air quality.

Although all the options, including the modeling without cumulus schemes, provided proper performance for modeling surface temperature, all of them, on average, overestimated this parameter between 13:00 and 17:00. This overestimation is consistent with the overestimation of the solar radiation at the surface, implying that in the urban area of Cuenca, the modeling of cloud dynamics needs to be improved. In the same way, although wind speed was acceptably modeled, all the options overestimated this parameter between 15:00 and 20:00. All the options demonstrated low performance for modeling wind direction, probably because of the complex topography of the region. An updated digital elevation model and land-use data would improve the modeling performance of wind direction.

The resolution of 1 km seems to allow for better modeling performance for precipitation over the urban area because of its less complex topography than the Cordillera. The anabatic winds from the valley, where the urban area is located, modulate the cloud formation and, therefore, define the precipitation levels over the Cordillera. The overestimation of computed precipitation for all the cumulus options used in this study would be improved using a more refined domain model over the Cordillera. In the future, an inner domain that combines a higher resolution (less than 1 km) over the Cordiller, with 1 km cells over the urban area can be assessed.

Published assessments about the influence of cumulus schemes at the grey zone mainly focused on precipitation modeling. We did not find studies covering meteorological and air quality variables for comparison purposes. Our findings over the urban area were consistent with Zhang et al. (2021) [35] (Table 12), who reported a clear improvement in modeling precipitation in the Central Great Plains of the United States without using a cumulus scheme at a 4 km resolution.

Similarly, Liang et al. (2019) [36] assessed the sensitivity for modeling rainfall in Jiangsu, China, to model configurations of grid nesting and convection treatment, using grid spacings from 30, 15, 9, 5, 3 to 1 km, concluding that convective parameterization in 30–9 km grids is required to represent organized cumuli, while explicitly resolving convections in cloud-permitting grids around 1 km is necessary to improve forecasts.

Amirudin et al. (2022) [37] performed simulations of precipitation over Peninsular Malaysia from 2013 to 2018 for assessing cumulus schemes at resolutions of 25, 5, and 1.6 km, reporting that at 5 km, the best-performing scheme was the Betts–Miller–Janjic. The finest resolution at 1.6 km simulation showed significant added value, as it was the only simulation to capture the high precipitation intensity in the morning and a precipitation peak during the evening. The authors indicated that cumulus schemes became less significant in a higher-resolution simulation.

Castorina et al. (2021) performed WRF simulations for modeling precipitation in Sicily (Italy) on 24 and 25 November 2016, working at 5 km [38]. The authors reported that using no cumulus schemes provided the most reliable and accurate solution with the highest accuracy. Other contributions, such as those of Wang et al. (2021) [39], who studied convection representation across the grey zone in forecasting warm-season extreme precipitation over Shanghai, reported that the use of cumulus schemes is beneficial at the 5 km grid resolution in simulating both powerful intensity and diurnal variations, although with mixed effects at 3 km. The primary rainfall peak at noon was best reproduced when the 1 km grid with explicit convection was nested directly into their outermost 15 km or 9 km grids using the Kain–Fritsch scheme. However, a secondary peak with a weak forcing was not detected.

Steeneveld and Peerlings (2020) [40] modeled a severe summer thunderstorm in the Netherlands, which took place on 3 June 2016, working at 4 and 2 km of resolution. They found that the Betts–Miller–Janjic scheme was activated too early and did not predict any convective system over the region of interest. The Grell–Freitas and Kain–Fritsch schemes predicted a convective system, but its intensity was underestimated. With the explicit convection, the model was able to resolve the storm. The authors indicated that modeling with the explicit convection (without cumulus scheme), the model captured the storm, although with a delay and an overestimated intensity.

On the contrary, other studies concluded that modeling in the grey zone without cumulus parameterization is inadequate. In this sense, Park et al. (2022) [41] performed WRF simulations with cumulus schemes and explicit convection (no convective parameterization) in South Korea, concluding that simulating convection processes using explicitly resolved convection leads to overestimations and erroneous precipitation locations.

Table 12. Summary of other assessments.

Area of Study	Period	Model	Resolution and Parameters	Main Findings	Source
Andean Region of Ecuador (Cuenca)	September 2014	WRF-Chem V3.2	1 km. Temperature, wind speed, wind direction, solar radiation, precipitation, air quality	No unique cumulus option was the best for modeling each of the assessed meteorological parameters. All the options provided comparable performances for modeling air quality variables. Deactivating the cumulus scheme could be beneficial for holistically modeling meteorological and air quality variables in the urban area of Cuenca.	This contribution
Central Great Plains, Eastern Kansas and western Missouri region (USA)	Three summers, from 2002 to 2004	NU-WRF	4 km. Precipitation	There was a clear improvement without using a cumulus scheme, which should become more evident with finer resolutions such as 1 km.	Zhang et al. (2021) [37]
Jiangsu, China	19 June to 20 July 2016	WRF-3.9	30, 15, 9, 5, 3, 1 km. Precipitation	Parameterization in 30–9 km grids is required to represent organized cumuli, while explicitly resolving convections in cloud-permitting grids around 1 km is necessary to improve forecasts.	Liang et al. (2019) [38]
Peninsular Malaysia	2013 to 2018	WRF	25, 5, 1.6 km. Precipitation	At 5 km, the best-performing scheme was the Betts–Miller–Janjic. The 1.6 km simulation showed significant improvement as it was the option that captured the high rainfall in the morning and a precipitation peak during the evening. The role of cumulus schemes became less significant in a higher-resolution simulation.	Amirudin et al. (2022) [39]
Andean Region of Ecuador (Cuenca)	1 to 11 November 2020	WRF-4.0.3	1 km. Temperature, wind speed, solar radiation	None of the cumulus options, including the deactivation of the cumulus scheme, adequately modeled the drop in temperature and solar radiation on 9 November 2020.	Parra (2022) [42]
Shanghai	25 May 2018, 10 June 2017	WRF	27, 15, 9, 5, 3, 1 km. Extreme precipitation	The primary rainfall peak at noon was best reproduced when the 1 km grid with explicit convection was nested directly into their outermost 15 km or 9 km grids using the Kain–Fritsch scheme. However, a secondary peak with a weak forcing was not detected.	Wang et al. (2021) [39]
Sicily (Italy)	24 to 25 November 2016	WRF	5 km. Precipitation	Using no cumulus schemes provided the most reliable and accurate solution with the highest accuracy.	Castorina et al. (2021) [38]
The Netherlands	23 to 24 June 2016	WRF 3.7.1	4, 2 km. Precipitation	Betts–Miller–Janjic activated too early and did not foresee any convective system. Grell–Freitas and Kain–Fritsch forecasted a convective system, but its intensity was underestimated. With the explicit convection (without cumulus scheme), the model resolved the storm, although with a delay and an overestimated intensity.	Steeneveld and Peerlings (2020) [40]
South Korea	15 to 16 July 2017	WRF	4 km. Extreme precipitation	Simulating convection processes in the grey zone without the convective parameterization scheme is inadequate.	Park et al. (2022) [41]
South Korea	26 to 27 July 2011	WRF	27, 9, 3, 1 km. Extreme precipitation	Multiple spurious cores occurred when the cumulus parameterization scheme was removed at 3 and 1 km of resolution.	Kwon and Hong (2017) [43]

Kwon and Hong (2017) [43] modeled a heavy rain event in South Korea using an updated version of a cumulus scheme and performed simulations with 3 and 1 km resolution without the cumulus option. They reported that an updated cumulus scheme outperformed the original version, and at 3 and 1 km, the precipitation core was well reproduced. On the contrary, multiple spurious cores occurred when the cumulus scheme was removed at those resolutions.

Our findings and the literature cited highlight the importance of dedicated studies to assess the effects of deactivating the cumulus parameterization on atmospheric modeling in the grey zone.

On average, CO levels were adequately modeled regarding air quality, especially from 06:00 to 10:00, suggesting that emissions and parameters involved in air dispersion, such as planetary boundary layer depth and atmospheric stability, were acceptably modeled during peak CO emissions. For other hours, CO levels were underestimated by about 0.5 mg m^{-3}. The overestimation of surface solar radiation and temperature around midday implies an overestimation of the planetary boundary layer depth during these hours and, therefore, the underestimation of CO concentrations.

On average, the hourly peak level of $PM_{2.5}$ was modeled at 08:00, two hours earlier than the records, which implies that the estimation of the hourly $PM_{2.5}$ emissions, especially from diesel cars, needs to be reviewed.

The overestimation of surface solar radiation implies a higher level of photochemical reactions that promote and partly explain the overestimation of the peak O_3. However, the generation and behavior of O_3 are more complex due to the participation of emissions of nitrogen oxides and volatile organic compounds under the influence of solar radiation. Overestimation of O_3 can also be contributed to by an inadequate estimation of emissions.

Based on the findings of the present contribution and from previous studies, we recommend the following reference configuration for atmospheric modeling over the urban area of Cuenca:

- Land use categories: Deduced from the USGS [3];
- Global atmospheric dataset for generation of initial and boundary conditions: FNL [21];
- Spatial resolution: 1 km (as per this contribution);
- Cumulus scheme: No cumulus option (as per this contribution);
- Land surface scheme: Noah [3];
- Urban Canopy Model: None [3];
- Planetary Boundary Layer: Yonsei University option [20];
- Chemical mechanisms and aerosol modules: CBMZ and MOSAIC with direct effects [20,23].

The indicated configuration would be useful for modeling meteorological and air quality variables over the urban area of Cuenca. However, as a limitation, this configuration and spatial resolution (1 km) will overestimate precipitation over the Cordillera. This configuration needs to be assessed for days with significant changes in meteorological conditions, such as a sudden drop in temperature and solar radiation, as of 9 November 2020, which was not adequately modeled by any of the cumulus options, including the deactivation of the cumulus scheme [42] (Table 12).

As all the options, including the deactivation of the cumulus scheme, overestimated the total amount of precipitation over the Cordillera, its modeling needs to be improved, particularly for studies on water supply, hydrological management, extreme rainfall events, and the influence of climate change. Hydropower energy is a critical component of the Ecuadorian mix generation and needs to be assessed correctly in terms of the influence of climate change [44]. Although all the options provided acceptable performances for air quality, the impact of modeled rainfall over the Cordillera and the overestimation of global solar radiation at the surface needs to be assessed, considering that emission inventory data has high uncertainties.

The reference configuration overestimated the computed rainfall, especially over the Cordillera, using all the cumulus schemes and deactivation, where daily precipitation up to 85 mm d^{-1} was computed. At the four stations of the Cordillera, MAN, VEN, IZH, and SOL, the maximum modeled daily rainfall reached 35.9, 49.6, 36.7, and 28.3 mm d^{-1}, respectively, although the corresponding maximum records were 20.1, 17.1, 15.1, and 14.1 mm d^{-1}. These results indicate that the reference configuration can indicate false alarms if used as an early warning system. For this purpose, a complete assessment of modeling rainfall is out of the scope of this manuscript, although it may be the focus of future research.

Having a reference configuration for atmospheric modeling in Cuenca will provide a powerful tool to validate future emission inventories, gain insights through the modeling approach about the effects on air quality due to changes in the current emissions sources, identify convenient locations, and assess the impact on future facilities that would contribute to their emissions.

This contribution provided insights for atmospheric modeling in the grey zone of spatial resolution over the Andean Region of Ecuador, highlighting the advantages and limitations of the cumulus options from WRF-Chem V3.2 and based on the principle that the modeling performance needs to be assessed for meteorological and air quality variables. The reference configuration could be the basis for a future atmospheric modeling tool to forecast variables, such as precipitation, temperature, $PM_{2.5,}$ and O_3 levels, based on the treatment of the atmosphere as a unique system, merging the objectives of the meteorological and air pollution communities, which currently primarily work from their sides. A future forecasting air quality system to help reduce air pollution's toll on public health [45].

Atmospheric modeling is particularly challenging in the Andean Region of Ecuador [46] because of the presence of the Andes, the dynamics of the ITCZ, and the breezes coming from the coastal and Amazonian regions. These factors promote convective movements with complex cloud dynamics, with division between the Pacific area west of the western Cordillera, with lower and more stratiform clouds, and the eastern parts, with an increased average cloud-top height towards the Amazon region [47].

The performance for modeling rainfall was investigated in this contribution based on daily intensities, through the ability of the model to capture days without and with rain. A more comprehensive assessment can incorporate a comparison between computed precipitation and records per precipitation ranges based on hourly intensities.

Although the availability of atmospheric records is low in the Andean Region of Ecuador [48,49], new assessments should include measurements from stations, such as from the western part of the urban area over the Cordillera chain, where the computed precipitation indicated that both convective (cumulus) and the microphysics components can be relevant. The Paute River basin, partially located in our study region, shows a high spatial rainfall and temperature variability [50,51]. In complex topography, numerical models also have shortcomings in capturing the distribution of rain with altitude [52]. Physics parameterization schemes have been developed and tested mainly for the Northern Hemisphere. The features of the Tropical Andean Region could demand the proposal of dedicated physics schemes to improve atmospheric modeling in this region.

The activation of indirect effects between meteorology and aerosols for modeling in the Andean Region is a component that deserves future research, which could improve the modeling of clouds and associated processes. Other elements need to be assessed, such as the microphysics parameterization, which determines the cloud life cycle and interaction between clouds and aerosols, affecting the solar radiation levels at the surface and rainfall processes. In addition, assessments of recent versions of WRF-Chem, other periods of dry and wet seasons, the data assimilation of records and remote sensing monitoring, and even the combination with artificial intelligence approaches are necessary.

Funding: This research was funded by the USFQ Poli-Grants 2024 program.

Institutional Review Board Statement: Not applicable.

Informed Consent Statement: Not applicable.

Data Availability Statement: Data are contained within the article.

Acknowledgments: This research is part of the "Emisiones atmosféricas y Calidad del Aire en el Ecuador 2024" project. Simulations were performed with the High-Performance Computing system at the Universidad San Francisco de Quito. The publication of this article was funded by the Universidad San Francisco de Quito USFQ Research Publication Fund. We thank EMOV EP and ETAPA EP, municipal entities that provided the meteorological and quality records. The publication of this article was funded by the Universidad San Francisco de Quito USFQ Research Publication Fund.

Conflicts of Interest: The author declares no conflicts of interest.

Appendix A

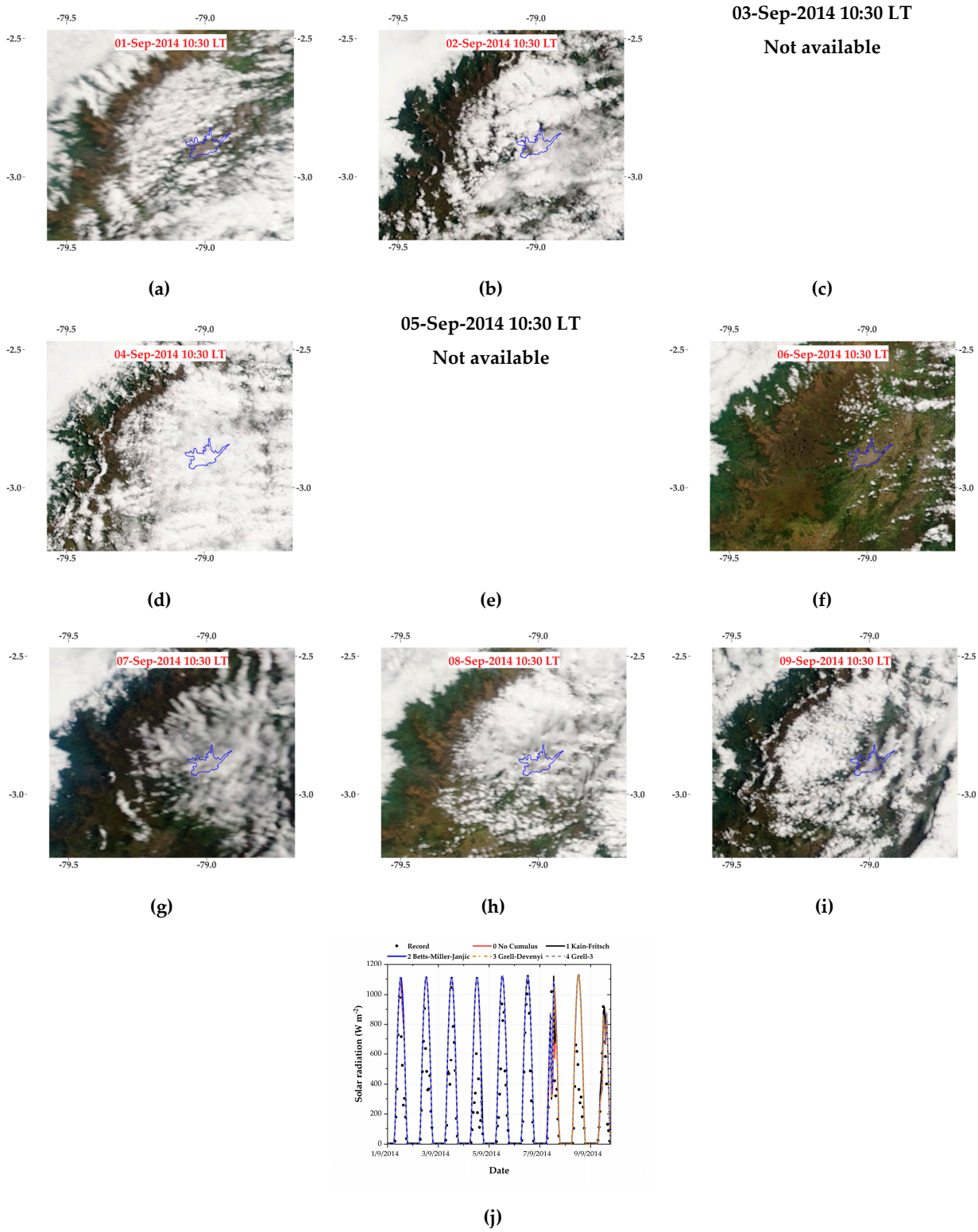


Figure A1. Images by the Terra satellite over Cuenca (10:30 LT) from (**a**–**i**) 01-Sep-2014–09-Sep-2014. respectivelly, the MUN station. (**j**) Global solar radiation records (W m^{-2}) and modeled results.

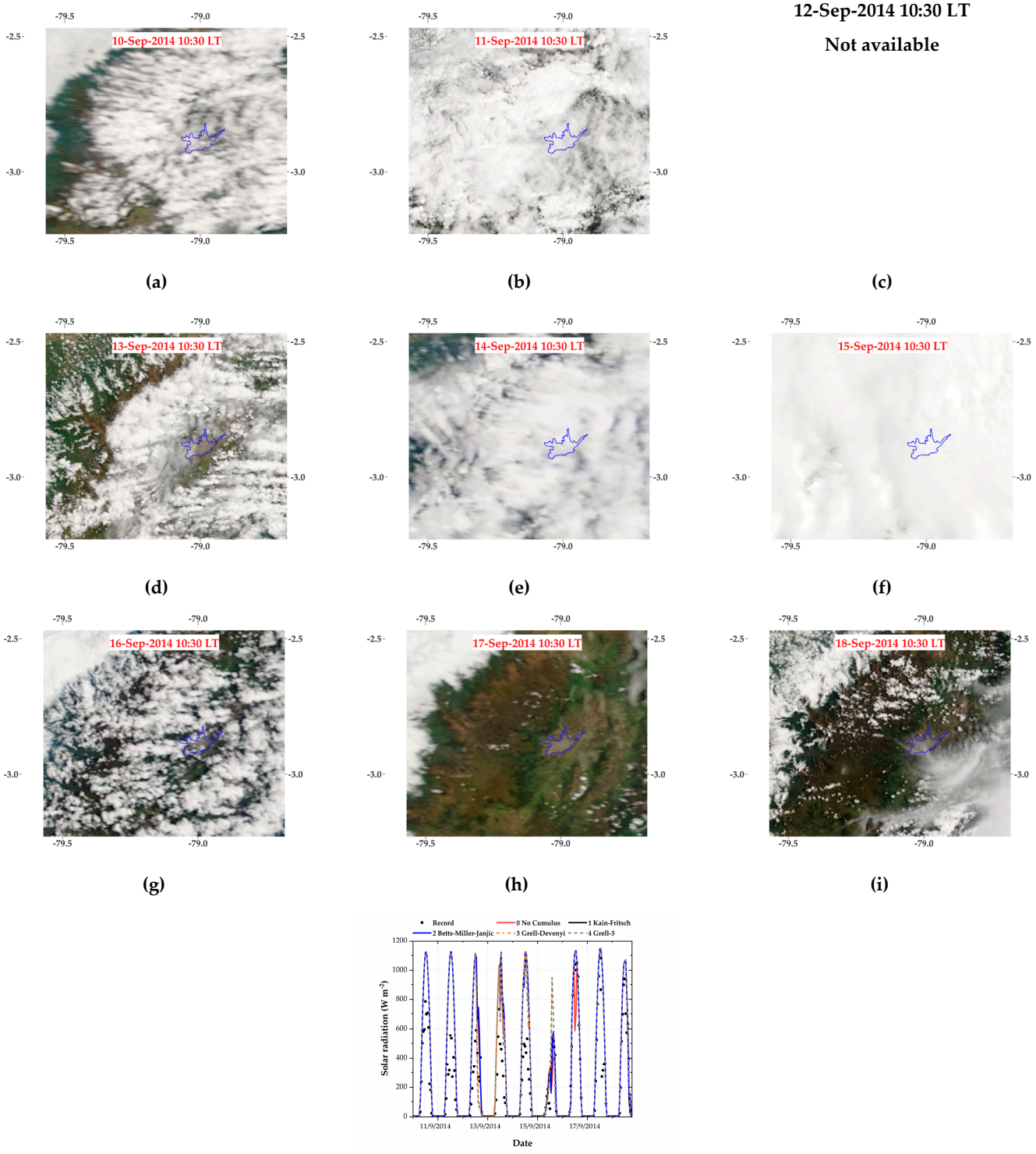


Figure A2. Images by the Terra satellite over Cuenca (10:30 LT) from (**a**–**i**) 10-Sep-2014–18-Sep-2014. respectivelly, the MUN station. (**j**) Global solar radiation records (W m^{-2}) and modeled results.

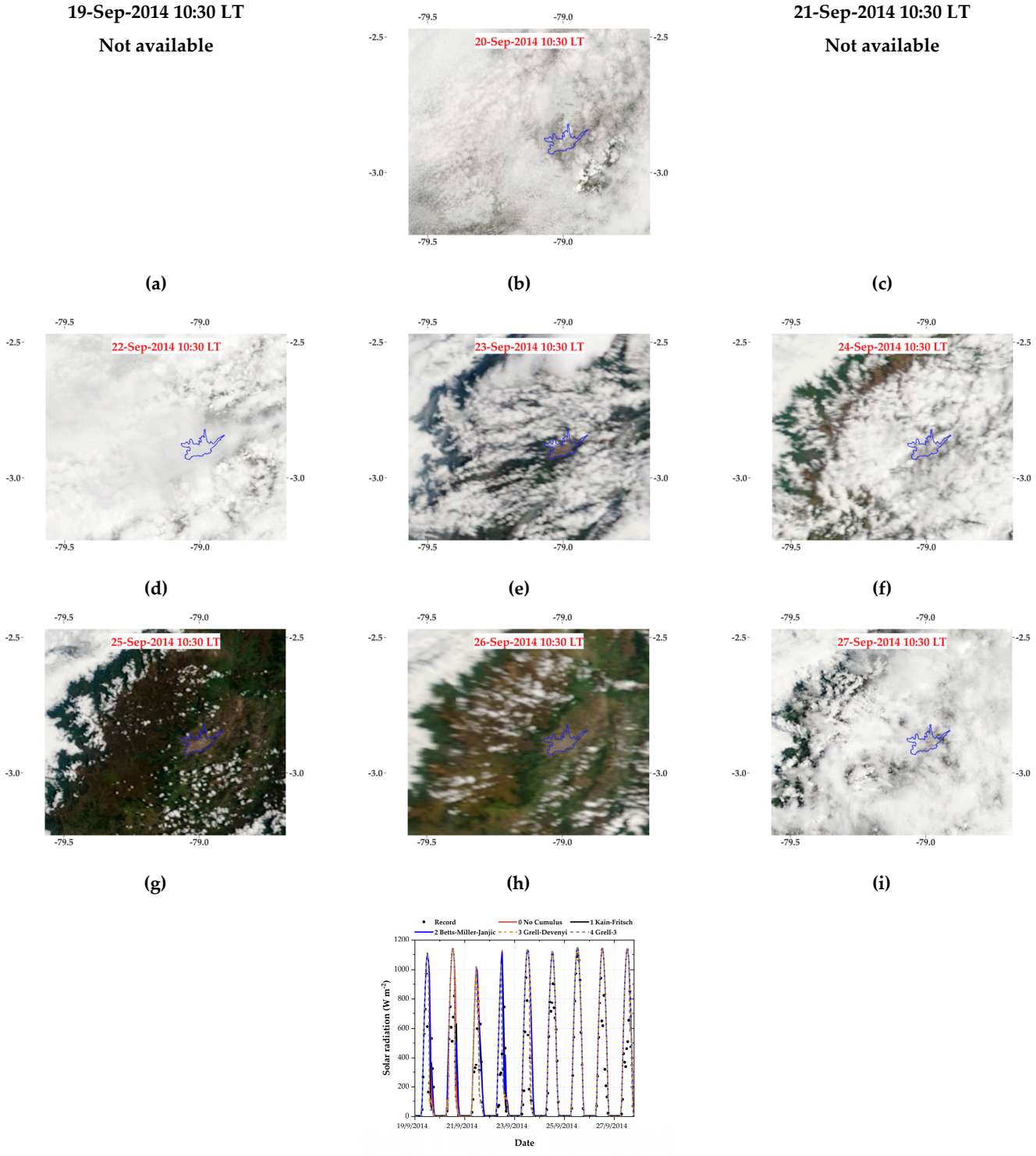


Figure A3. Images by the Terra satellite over Cuenca (10:30 LT) from (**a**–**i**) 19-Sep-2014–27-Sep-2014. respectivelly, the MUN station. (**j**) Global solar radiation records (W m^{-2}) and the corresponding modeled results.

Table A1. Cloudy conditions in Cuenca from 1-Sep-2014 to 27-Sep-2014 and qualitative performance for modeling global solar radiation at the surface by the cumulus options.

Date	Cloud Conditions [1]	Cumulus Option				
		0 No Cumulus	1 Kain–Fritsch	2 Betts–Miller–Janjic	3 Grell–Devenyi	4 Grell-3
01-Sep-2014	Partly cloudy	Overestimated	Overestimated	Overestimated	Overestimated	Overestimated
02-Sep-2014	Partly cloudy	Overestimated	Overestimated	Overestimated	Overestimated	Overestimated
03-Sep-2014	-	Overestimated	Overestimated	Overestimated	Overestimated	Overestimated
04-Sep-2014	Partly cloudy	Overestimated	Overestimated	Overestimated	Overestimated	Overestimated
05-Sep-2014	-	Overestimated	Overestimated	Overestimated	Overestimated	Overestimated
06-Sep-2014	Cloudless	Acceptable	Acceptable	Acceptable	Acceptable	Acceptable
07-Sep-2014	Partly cloudy	Acceptable	Acceptable	Acceptable	Acceptable	Acceptable
08-Sep-2014	Partly cloudy	Overestimated	Overestimated	Overestimated	Overestimated	Overestimated
09-Sep-2014	Partly cloudy	Acceptable	Acceptable	Acceptable	Acceptable	Acceptable
10-Sep-2014	Partly cloudy	Overestimated	Overestimated	Overestimated	Overestimated	Overestimated
11-Sep-2014	Partly cloudy	Overestimated	Overestimated	Overestimated	Overestimated	Overestimated
12-Sep-2014	-	Overestimated	Overestimated	Overestimated	Overestimated [2]	Overestimated [2]
13-Sep-2014	Partly cloudy	Overestimated	Overestimated	Overestimated	Overestimated	Overestimated
14-Sep-2014	Cloudy	Overestimated	Overestimated	Overestimated	Overestimated	Overestimated
15-Sep-2014	Cloudy	Acceptable [2]	Acceptable [2]	Acceptable [2]	Acceptable	Acceptable
16-Sep-2014	Partly cloudy	Acceptable [3]	Acceptable	Acceptable	Acceptable	Acceptable
17-Sep-2014	Cloudless	Acceptable [4]	Acceptable [4]	Acceptable [4]	Acceptable [4]	Acceptable[4]
18-Sep-2014	Cloudless	Acceptable	Acceptable	Acceptable	Acceptable	Acceptable
19-Sep-2014	-	Acceptable [4]	Acceptably [4]	Acceptably [4]	Acceptably [4]	Acceptably [4]
20-Sep-2014	Cloudy	Acceptable [5]	Acceptably [5]	Acceptably [5]	Acceptably [5]	Acceptably [5]
21-Sep-2014	-	Overestimated [2]	Overestimated [2]	Overestimated [2]	Overestimated [2]	Overestimated [2]
22-Sep-2014	Cloudy	Overestimated [2]	Overestimated [2]	Overestimated [2]	Overestimated [2]	Overestimated [2]
23-Sep-2014	Partly cloudy	Overestimated	Overestimated	Overestimated	Overestimated [2]	Overestimated [2]
24-Sep-2014	Partly cloudy	Acceptably [5]	Acceptable [5]	Acceptably [5]	Acceptably [5]	Acceptable [5]
25-Sep-2014	Cloudless	Acceptable	Acceptable	Acceptable	Acceptable	Acceptable
26-Sep-2014	Cloudless	Acceptably [4]	Acceptably [4]	Acceptably [4]	Acceptably [4]	Acceptable [4]
27-Sep-2014	Partly cloudy	Overestimated	Overestimated	Overestimated	Overestimated	Overestimated

1: Based on images from the Terra satellite (10:30 LT) [33]. 2: Better modeled during the afternoon. 3: Underestimated around midday. 4: Overestimated during the afternoon. 5: Overestimated around midday.

References

1. Baklanov, A.; Schlünzen, K.; Suppan, P.; Baldasano, J.; Brunner, D.; Aksoyoglu, S.; Carmichael, G.; Douros, J.; Flemming, J.; Forkel, R.; et al. Online Coupled Regional Meteorology Chemistry Models in Europe: Current Status and Prospects. *Atmos. Chem. Phys.* **2014**, *14*, 317–398. [CrossRef]
2. Atmosphere | Free Full-Text | Crossing Multiple Gray Zones in the Transition from Mesoscale to Microscale Simulation over Complex Terrain. Available online: https://www.mdpi.com/2073-4433/10/5/274 (accessed on 15 October 2023).
3. Parra, R. Assessment of Land Surface Schemes from the WRF-Chem for Atmospheric Modeling in the Andean Region of Ecuador. *Atmosphere* **2023**, *14*, 508. [CrossRef]
4. Skamarock, W.C.; Klemp, J.B.; Dudhia, J.; Gill, D.O.; Barker, D.M.; Duda, M.G.; Huang, X.-Y.; Wang, W.; Powers, J.G. *A Description of the Advanced Research WRF Version 3*; University Corporation for Atmospheric Research: Boulder, CO, USA, 2008.
5. Grey Zone Project for Model Parameterizations. Met Office. Available online: https://www.metoffice.gov.uk/research/approach/collaboration/grey-zone-project (accessed on 18 November 2023).
6. Kealy, J.C. Probing the 'Grey Zone' of NWP—Is Higher Resolution Always Better? *Weather* **2019**, *74*, 246–249. [CrossRef]
7. Warner, T.T. *Numerical Weather and Climate Prediction*; Cambridge University Press: Cambridge, UK, 2010. [CrossRef]
8. Kain, J.S. The Kain–Fritsch Convective Parameterization: An Update. *J. Appl. Meteorol. Climatol.* **2004**, *43*, 170–181. [CrossRef]
9. Janjić, Z.I. The Step-Mountain Eta Coordinate Model: Further Developments of the Convection, Viscous Sublayer, and Turbulence Closure Schemes. *Mon. Weather Rev.* **1994**, *122*, 927–945. [CrossRef]
10. Janjić, Z.I. Comments on "Development and Evaluation of a Convection Scheme for Use in Climate Models". *J. Atmos. Sci.* **2000**, *57*, 3686. [CrossRef]
11. Grell, G.A.; Dévényi, D. A Generalized Approach to Parameterizing Convection Combining Ensemble and Data Assimilation Techniques. *Geophys. Res. Lett.* **2002**, *29*, 38-1–38-4. [CrossRef]
12. Grell, G.A. Prognostic Evaluation of Assumptions Used by Cumulus Parameterizations. *Mon. Weather Rev.* **1993**, *121*, 764–787. [CrossRef]
13. Stensrud, D. *Parameterization Schemes: Keys to Understanding Numerical Weather Prediction Models*; Cambridge University Press: New York, NY, USA, 2009.
14. Baklanov, A.; Brunner, D.; Carmichael, G.; Flemming, J.; Freitas, S.; Gauss, M.; Hov, Ø.; Mathur, R.; Schlünzen, K.H.; Seigneur, C.; et al. Key Issues for Seamless Integrated Chemistry–Meteorology Modeling. *Bull. Am. Meteorol. Soc.* **2017**, *98*, 2285–2292. [CrossRef]

15. Molina, C.; Caguana, C.; Heredia, E.; Parra, R. *Informe de La Calidad Aire Cuenca 2022*; Alcaldía de Cuenca. Red de Monitoreo de la EMOV EP: Cuenca, Ecuador, 2023.
16. World Health Organization. *WHO Global Air Quality Guidelines: Particulate Matter (PM2.5 and PM10), Ozone, Nitrogen Dioxide, Sulfur Dioxide and Carbon Monoxide*; World Health Organization: Geneva, Switzerland, 2021.
17. Phalen, R.F.; Phalen, R.N. *Introduction to Air Pollution Science: A Public Health Perspective*; Jones & Bartlett Publishers: Burlington, MA, USA, 2013.
18. Parra, R. *Inventario de Emisiones Atmosféricas Del Cantón Cuenca 2014*; EP Petroecuador: Cuenca, Ecuador, 2016. [CrossRef]
19. Parra, R. Performance Studies of Planetary Boundary Layer Schemes in WRF-Chem for the Andean Region of Southern Ecuador. *Atmos. Pollut. Res.* **2018**, *9*, 411–428. [CrossRef]
20. WRF Model Users Site. Available online: https://www2.mmm.ucar.edu/wrf/users/ (accessed on 30 December 2022).
21. CISL RDA: NCEP FNL Operational Model Global Tropospheric Analyses, Continuing from July 1999. Available online: https://rda.ucar.edu/datasets/ds083.2/ (accessed on 30 December 2022).
22. Zaveri, R.A.; Peters, L.K. A New Lumped Structure Photochemical Mechanism for Large-Scale Applications. *J. Geophys. Res.* **1999**, *104*, 30387–30415. [CrossRef]
23. Zaveri, R.A.; Easter, R.C.; Fast, J.D.; Peters, L.K. Model for Simulating Aerosol Interactions and Chemistry (MOSAIC). *J. Geophys. Res.* **2008**, *113*, D13204. [CrossRef]
24. Hong, S.-Y.; Dudhia, J.; Chen, S.-H. A Revised Approach to Ice Microphysical Processes for the Bulk Parameterization of Clouds and Precipitation. *Mon. Weather Rev.* **2004**, *132*, 103–120. [CrossRef]
25. Mlawer, E.J.; Taubman, S.J.; Brown, P.D.; Iacono, M.J.; Clough, S.A. Radiative Transfer for Inhomogeneous Atmospheres: RRTM, a Validated Correlated-k Model for the Longwave. *J. Geophys. Res.* **1997**, *102*, 16663–16682. [CrossRef]
26. Chou, M.-D.; Suarez, M.J. *A Solar Radiation Parameterization for Atmospheric Studies*; NASA/TM-1999-104606/VOL15; NASA: Washington, DC, USA, 1999. Available online: https://ntrs.nasa.gov/citations/19990060930 (accessed on 30 December 2022).
27. Paulson, C.A. The Mathematical Representation of Wind Speed and Temperature Profiles in the Unstable Atmospheric Surface Layer. *J. Appl. Meteor.* **1970**, *9*, 857–861. [CrossRef]
28. Hong, S.-Y.; Noh, Y.; Dudhia, J. A New Vertical Diffusion Package with an Explicit Treatment of Entrainment Processes. *Mon. Weather Rev.* **2006**, *134*, 2318–2341. [CrossRef]
29. Chen, F.; Dudhia, J. Coupling an Advanced Land Surface–Hydrology Model with the Penn State–NCAR MM5 Modeling System. Part II: Preliminary Model Validation. *Mon. Weather Rev.* **2001**, *129*, 587–604. [CrossRef]
30. The Application of Models under the European Union's Air Quality Directive: A Technical Reference Guide—European Environment Agency. Available online: https://www.eea.europa.eu/publications/fairmode (accessed on 30 December 2022).
31. Simon, H.; Baker, K.R.; Phillips, S. Compilation and Interpretation of Photochemical Model Performance Statistics Published between 2006 and 2012. *Atmos. Environ.* **2012**, *61*, 124–139. [CrossRef]
32. Rain Day—Glossary of Meteorology. Available online: https://glossary.ametsoc.org/wiki/Rain_day (accessed on 21 November 2023).
33. EOSDIS Worldview. Available online: https://worldview.earthdata.nasa.gov/?lg=false&t=2023-12-04-T23:48:40Z (accessed on 4 December 2023).
34. World Health Organization. *Regional Office for Europe. Air Quality Guidelines for Europe*; World Health Organization. Regional Office for Europe: Copenhagen, Denmark, 2000.
35. Zhang, Y.; Roundy, J.K.; Santanello, J.A. Evaluating the Impact of Model Resolutions and Cumulus Parameterization on Precipitation in NU-WRF: A Case Study in the Central Great Plains. *Environ. Model. Softw.* **2021**, *145*, 105184. [CrossRef]
36. Liang, X.-Z.; Li, Q.; Mei, H.; Zeng, M. Multi-Grid Nesting Ability to Represent Convections Across the Gray Zone. *J. Adv. Model. Earth Syst.* **2019**, *11*, 4352–4376. [CrossRef]
37. Amirudin, A.A.; Salimun, E.; Zuhairi, M.; Tangang, F.; Juneng, L.; Mohd, M.S.F.; Chung, J.X. The Importance of Cumulus Parameterization and Resolution in Simulating Rainfall over Peninsular Malaysia. *Atmosphere* **2022**, *13*, 1557. [CrossRef]
38. Castorina, G.; Caccamo, M.T.; Colombo, F.; Magazù, S. The Role of Physical Parameterizations on the Numerical Weather Prediction: Impact of Different Cumulus Schemes on Weather Forecasting on Complex Orographic Areas. *Atmosphere* **2021**, *12*, 616. [CrossRef]
39. Wang, R.; Qiao, F.; Liang, X.-Z.; Zhu, Y.; Zhang, H.; Li, Q.; Ding, Y. Role of Convection Representation across the Gray Zone in Forecasting Warm Season Extreme Precipitation over Shanghai from Two Typical Cases. *Atmos. Res.* **2021**, *253*, 105370. [CrossRef]
40. Steeneveld, G.-J.; Peerlings, E.E.M. Mesoscale Model Simulation of a Severe Summer Thunderstorm in The Netherlands: Performance and Uncertainty Assessment for Parameterised and Resolved Convection. *Atmosphere* **2020**, *11*, 811. [CrossRef]
41. Park, H.; Kim, G.; Cha, D.-H.; Chang, E.-C.; Kim, J.; Park, S.-H.; Lee, D.-K. Effect of a Scale-Aware Convective Parameterization Scheme on the Simulation of Convective Cells-Related Heavy Rainfall in South Korea. *J. Adv. Model. Earth Syst.* **2022**, *14*, e2021MS002696. [CrossRef]
42. Parra, R. *Assessment of Cumulus Parameterization Schemes in Modeling Meteorology Associated with an Air Pollution Event in the Andean Region of Ecuador*; WIT Press: Milan, Italy, 2022; pp. 3–14. [CrossRef]
43. Kwon, Y.C.; Hong, S.-Y. A Mass-Flux Cumulus Parameterization Scheme across Gray-Zone Resolutions. *Mon. Weather Rev.* **2017**, *145*, 583–598. [CrossRef]

44. Naranjo-Silva, S. A Hydropower Development Perspective in Ecuador: Past, Present, and Future. *La Granja* **2024**, *39*, 63–77. [CrossRef]
45. Kumar, R.; Peuch, V.-H.; Crawford, J.H.; Brasseur, G. Five Steps to Improve Air-Quality Forecasts. *Nature* **2018**, *561*, 27–29. [CrossRef] [PubMed]
46. Tobar, V.; Wyseure, G. Seasonal Rainfall Patterns Classification, Relationship to ENSO and Rainfall Trends in Ecuador. *Int. J. Climatol.* **2018**, *38*, 1808–1819. Available online: https://rmets.onlinelibrary.wiley.com/doi/abs/10.1002/joc.5297 (accessed on 21 December 2023). [CrossRef]
47. Bendix, J.; Rollenbeck, R.; Göttlicher, D.; Cermak, J. Cloud Occurrence and Cloud Properties in Ecuador. *Clim. Res.* **2006**, *30*, 133–147. [CrossRef]
48. Cazorla, M.; Parra, R.; Herrera, E.; da Silva, F.R. Characterizing Ozone throughout the Atmospheric Column over the Tropical Andes from in Situ and Remote Sensing Observations. *Elem. Sci. Anthr.* **2021**, *9*, 00019. [CrossRef]
49. Rainfall and Cloud Dynamics in the Andes: A Southern Ecuador Case Study. Available online: https://www.hindawi.com/journals/amete/2016/3192765/ (accessed on 21 December 2023).
50. Celleri, R.; Willems, P.; Buytaert, W.; Feyen, J. Space–Time Rainfall Variability in the Paute Basin, Ecuadorian Andes. *Hydrol. Process.* **2007**, *21*, 3316–3327. [CrossRef]
51. Mora, D.E.; Willems, P. Decadal Oscillations in Rainfall and Air Temperature in the Paute River Basin—Southern Andes of Ecuador. *Theor. Appl. Climatol.* **2012**, *108*, 267–282. [CrossRef]
52. Ban, N.; Schmidli, J.; Schär, C. Evaluation of the Convection-Resolving Regional Climate Modeling Approach in Decade-Long Simulations. *J. Geophys. Res. Atmos.* **2014**, *119*, 7889–7907. [CrossRef]

Disclaimer/Publisher's Note: The statements, opinions and data contained in all publications are solely those of the individual author(s) and contributor(s) and not of MDPI and/or the editor(s). MDPI and/or the editor(s) disclaim responsibility for any injury to people or property resulting from any ideas, methods, instructions or products referred to in the content.